Article

Poly(amidoamine) Dendrimer-Doxorubicin Conjugates: In vitro characteristics and Pseudo-Solution Formulation in Pressurized Metered-Dose Inhalers

Qian Zhong, and Sandro R. P. da Rocha

Mol. Pharmaceutics, **Just Accepted Manuscript** • DOI: 10.1021/acs.molpharmaceut.5b00876 • Publication Date (Web): 01 Feb 2016

Poly(amidoamine) Dendrimer-Doxorubicin Conjugates: *In vitro* characteristics and Pseudo-Solution Formulation in Pressurized Metered-Dose Inhalers

Qian Zhong[1] and Sandro R. P. da Rocha[1,2*]

[1]Department of Chemical Engineering and Materials Science, College of Engineering, Wayne State University, 5050 Anthony Wayne Drive, Detroit, Michigan 48202, United States

[2]Pharmaceutics and Chemical and Life Science Engineering, Virginia Commonwealth University, 410 N 12th Street, Richmond, Virginia, 23298-0533, United States

To whom correspondence should be addressed: srdarocha@vcu.edu; Phone: +1 (804) 828-0985

Abstract

Lung cancers are the leading cause of cancer death for both men and women. A series of PEGylated poly(amidoamine) dendrimer-based doxorubicin (DOX) nanocarriers ($G3NH_2$-mPEG-nDOX) were synthesized and their chemistry tailored for the development of novel pseudo-solution formulations in propellant-based metered-dose inhalers (pMDIs) with enhanced aerosol characteristics. A pH-labile bond was used to conjugate DOX to dendrimer for controlled intracellular release. We employed a two-step PEGylation strategy to cover a range of DOX loading and PEGylation density. We investigated the impact of pH, PEGylation density and DOX payload on the release of DOX from the conjugate. We also determined the cellular internalization of the conjugate, the intracellular release kinetics of DOX from the conjugate, and their ability to kill human alveolar carcinoma cells (A549). The acid-labile conjugates sustained the release of DOX in acidic medium, and also intracellularly, as determined by nuclear co-localization studies with confocal microscopy. Meanwhile, DOX was retained in the conjugate at extracellular physiological conditions, indicating their potential to achieve spatial and temporal controlled release profiles. We also observed that the kinetics of cellular entry of the conjugates with DOX increased significantly compared to free DOX. Due to controlled release, the $G3NH_2$-mPEG-nDOX conjugates showed time-dependent cell kill, but their cell kill ability was comparable to free DOX, which suggests their potential *in vivo* as compared to free DOX. The conjugates were formulated in pMDIs as pseudo-solution formulations, with the help of a minimum amount of cosolvent (ethanol; <0.4%; v/v). The physical stability and aerosol characteristics of the conjugates were controlled by the PEGylation density of the carriers – the higher the PEG density the better the dispersibility and the better the deep lung deposition of the conjugates (fine particle fraction up to ca. 80%).

Keywords: polyamidoamine dendrimer (PAMAM), doxorubicin, lung cancer, pressurized metered-dose inhalers, controlled release.

1. Introduction

Cancer is the second most common cause of death in the United States.[1, 2] An estimated 1.7 million new cases are diagnosed yearly, with ca. 600 thousand cancer deaths.[3] Among the many types of malignant tumors, lung cancers are of great relevance as they are the leading cause of cancer death among both men and women.[4, 5] More people die of lung cancer than colorectal, breast, pancreatic, and prostate cancers combined.[1]

Chemotherapy is widely used in the fight against primary lung cancers and lung metastasis.[6-9] However, there are several limitations in using chemotherapeutics to treat lung cancers. One major challenge is the low chemotherapeutic concentration found in the lung tumor upon intravenous (i.v.) administration.[8, 10] It is estimated that only a few percent (ca. 2-4%) of the total dose administered i.v. reaches the lung tumor.[11] Dose limiting toxicity is another major issue in the chemotherapeutic treatment of lung cancers.[12] This problem is compounded as high i.v. dosages are usually required due to the poor distribution profile of chemotherapeutics.[11]

Doxorubicin (DOX) is a leading therapeutic in clinical oncology, having a broad range of activity against both "liquid" and solid tumors,[13] including lung cancers.[8, 14, 15] Since the discovery of DOX, thousands of other anthracyclines have been screened for their anticancer properties, but only few have emerged as clinically relevant.[16] In spite of its immense acceptability, however, DOX causes a series of side effects, of particularly relevance being its toxicity to the cardiac tissue.[17-19] While DOX-induced cardiomyopathy is clinically manageable, it is associated with 50% mortality in those patients that develop congestive heart failure during treatment,[20, 21] thus limiting the range of applicability of this powerful therapeutic. The ability to efficiently deliver DOX locally to the lungs, and to improve DOX's biodistribution by minimizing its concentration in the

cardiac tissue may, therefore, represent an important step forward in the use of such a relevant anti-cancer therapeutic in the treatment of lung cancers.

Nanocarriers have the potential to improve the biodistribution and pharmacokinetic profiles of various therapeutics including anti-cancer drugs.[22-25] Dendrimers are particularly relevant nanocarrier systems as they are highly monodisperse,[26] have a large number of surface groups amenable to the conjugation of therapeutic molecules and also other agents and ligands that allow for the enhancement of the properties of the nanocarriers such as increased aqueous solubility upon conjugation of hydrophobic therapeutics[27] (as is the case for DOX), and enhanced pharmacokinetic and biodistribution profiles,[28] as well as the tagging of imaging agents for theranostics,[29, 30] among others. Particularly relevant to this work is the fact that we have also recently shown that the chemistry of generation 3, amine-terminated PAMAM dendrimers ($G3NH_2$) can be used to modulate their interaction with the pulmonary epithelium both *in vitro* and *in vivo*,[31] and can thus be potentially used to improve therapeutic outcomes of DOX.

Based on the challenges and opportunities discussed above, the goal of this work was to evaluate the interaction of PAMAM dendrimer-DOX conjugates with an *in vitro* lung cancer model, and to develop portable oral inhalation (OI) formulations for the local delivery of the DOX conjugates to the lungs. More specifically, we propose to synthesize and characterize $G3NH_2$-DOX conjugates with an intracellular degradable linker and varying densities of PEG 1000Da, and to evaluate the kinetics of cellular internalization, intracellular DOX release and organelle colocalization, and cell kill on A549 cells – a model of the alveolar epithelial human adenocarcinoma. Moreover, we also propose to develop HFA-based pMDI formulations of the $G3NH_2$-DOX conjugates with aerosol characteristics conducive to deep lung deposition of DOX.

2. Materials

Generation 3, amine-terminated, poly(amido amine) (PAMAM) dendrimer ($G3NH_2$, 32 - NH_2 surface groups, theoretical molecular weight = 6909) was purchased from Dendritech, Inc (Miland, MI, USA). PEG1000 Da succinimidyl ester (PEG1K-SE) was purchased from NANOCS Inc (New York, NY, USA). Doxorubicin hydrochloride salt (DOX; research grade; purity > 99%) was purchased from LC Laboratories (Woburn, MA, USA). Cis-aconityl anhydride, succinic anhydride, triethylamine (TEA), 2, 5-dihydoxybenzoic acid (2, 5-DHB), ethyl-3-(3-dimethylaminopropyl) carbodiimide (EDC) and N-hydroxylsuccinimide (NHS) were purchased from Sigma-Aldrich (St Louis, MO, USA). 3-(4, 5-dimethylthiazol-2-yl)-2, 5-diphenyltetrazolium bromide (MTT) was purchased from Life Technologies (Grand Island, NY, USA). Deuterated dimethylsulfoxide ($DMSO\_d_6$) was purchased from Cambridge Isotope Laboratories (Andover, MA, USA). Ultrapure deionized water (DI H_2O, Ω=18.0-18.2) was sourced from a Barnstead NANOpure DIamond System (D11911), equipment purchased from Thermo Fisher Scientific (Waltham, MA, USA). 1,1,1,2,3,3,3-heptafluoropropane (HFA227) with trade name Dupont™ FM-200® and 2H, 3H perfluoropentane (HPFP) with trade name Vertrel™ XF were purchased from Dupont (Wilmington, DE, USA). A549 human lung cancer cell line was purchased from American Type Culture Collection (Manassas, VA, USA). Spectra®Por dialysis membrane (MWCO = 3000Da) was purchased from Spectrum Laboratories, Inc (Rancho Dominguez, CA, USA). Amicon® Ultra 15 centrifugal filter device (MWCO = 3000Da) was purchased from EMD Millipore (Billerica, MA, USA). Thin layer chromatography (TLC) Silica gel 60 F_{254} plastic sheet was purchased from Merck KGaA (Darmstadt, Germany). All reagents were used as received unless specified elsewhere.

3. Methods

3.1. Synthesis and characterization of acid-labile, PEGylated PAMAM-DOX conjugates (G3NH$_2$-mPEG-nDOX). As shown in Figure 1, DOX was reacted with cis-aconityl anhydride in basic aqueous solution to obtain cis-aconityl DOX. Acid-labile, PEGylated conjugates were synthesized via two different routes: *Direct PEGylation* or *Two-step PEGylation*. In the *Direct PEGylation* approach, cis-aconityl DOX was first conjugated to G3NH$_2$ using EDC/NHS chemistry. PEG was subsequently conjugated to G3NH$_2$-nDOX to obtain the final product G3NH$_2$-mPEG-nDOX. Various PEG densities (m = 0, 9 and 21) were achieved by reacting different ratios of PEG-SE to G3NH$_2$-nDOX. The *Two-step PEGylation* strategy was required in order to achieve higher payloads of DOX (in this particular case for n = 7), as G3NH$_2$-nDOX becomes too hydrophobic and crashes out of solution for n > 3. In the *Two-step PEGylation* strategy, G3NH$_2$ is first pre-PEGylated at a low/medium PEG density. Cis-aconityl DOX is subsequently conjugated (to a high/desired payload) to the pre-PEGylated dendrimer using EDC/NHS chemistry. Finally, additional PEG is conjugated onto the pre-PEGylated dendrimer-DOX conjugates, so as to achieve the desired/final PEG density. Proton nuclear magnetic resonance (^{1}H NMR) was recorded using Mercury 400 spectrometer (Agilent Technologies, Inc. Santa Clara, CA, USA). The molecular weight (MW) of the various intermediates and final products was determined by electrospray ionization (ESI) mass spectrometry using a ZQ-Waters TERS/Micromass spectrometer (Waters Corporation. Milford, MA, USA) and matrix-assisted laser desorption ionization-time of flight (MALDI-TOF) using a Bruker Daltonics UltrafleXtreme mass spectrometer (Bruker Corporation. Billerica, MA, USA). Hydrodynamic diameter (HD) and zeta potential (ζ) were determined using Zetasizer Nano ZS (Malvern Instruments Ltd. Malvern, Worcestershire, UK). Solvated diameter

(SD) was also determined using the Zetasizer Nano ZS, but in that case in HPFP (non-aqueous solvent). Detailed procedures for these measurements are described in ***Supporting Information S1***. All synthetic details of the conjugates are also described in ***Supporting Information S2***.

3.2. Synthesis and characterization of non-labile, PEGylated PAMAM-DOX conjugates (G3NH$_2$-mPEG-nDOXNL). The non-labile G3NH$_2$-mPEG-nDOXNL conjugates were synthesized via the same strategy—direct PEGylation and two-step PEGylation—as described in ***Section 3.1***. The only one difference is that DOX was first reacted with succinic anhydride in non-aqueous solution. The term "non-labile" denotes a covalent bond between DOX and G3NH$_2$ is stable at both intracellular and extracellular/physiological environment.

3.3. Culture of A549 Cells. Human lung alveolar adenocarcinoma epithelia cells (A549), passages 10 to 15, were plated in 75 cm^2 Corning™ cell culture treated flask (canted neck and vented cap) at a density of 10^4 cells/mL, and cultured with Dulbecco's Modified Eagle's Medium (DMEM, Life Technologies) supplemented with 10% Fetal Bovine Serum (FBS, Atlanta Biologicals) and penicillin (100 U/ml)-streptomycin (100 μg/ml) (Pen-Strep. Life Technologies). The cells were grown in Thermo Scientific™ CO_2 incubator (Thermo Fisher Scientific) at 37 ^oC and 5% CO_2. The medium was exchanged every two days and the cells were split when they reached ca. 80% confluence.

3.4. *In vitro* release of acid-labile G3NH$_2$-mPEG-nDOX and acid-non-labile G3NH$_2$-mPEG-nDOXNL conjugates. *In vitro* release was determined at both pH 7.4 and 4.5, representing the extracellular physiological pH and the lysosomal pH, respectively. DOX is chemically stable at pHs above 3.[32, 33] For the release studies at pH 7.4, 2 mL phosphate buffer saline (PBS, 1X, pH 7.4) containing free DOX or the conjugates (all with 0.38 μmol DOX or equiv.) was initially added to a

dialysis membrane (MWCO = 3000Da). The dialysis membrane was subsequently immersed in a capped glass beaker with 30 mL PBS – sink conditions. Citrate buffer (10 mM, pH 4.5) was used as buffer solution inside and outside dialysis membrane for release at pH 4.5. The *in vitro* release studies were performed in MaxQ thermostatic water bath shaker (Thermo Fisher Scientific), preset to 37.0±0.2 °C. A 0.1 mL solution from outside the dialysis bag was sampled at predetermined time points, and the concentration of DOX was determined by measuring absorption at 490 nm using a Biotek Synergy 2 Multi-Mode Microplate Reader (Biotek Instruments, Inc. Winnooski, VT, USA). The samples were returned to the outside buffer solution after each time point. These experiments were run in triplicate. The cumulative release of DOX from G3NH_2-mPEG-nDOX and G3NH_2-mPEG-nDOXNL was plotted as a function of time.

3.5. Cell kill of acid-labile G3NH_2-mPEG-nDOX and acid-non-labile G3NH_2-mPEG-nDOXNL conjugates. The ability of DOX, G3NH_2-mPEG, G3NH_2-mPEG-nDOX, and G3NH_2-mPEG-nDOXNL conjugates to kill A549 lung cancer cells was assessed using the MTT assay. A series of concentrations were sterilized by filtering sample-laden DMEM (no phenol red) through 0.22 μm sterile syringe filter (VWR Internationals. Radnor, PA, USA). 1×10^4 cells/well (n=8 per concentration) were seeded in tissue culture treated 96-well plate (VWR Internationals) with DMEM (no phenol red). The medium was removed after 24 h, and 100 μL of the sample-laden DMEM (no phenol red) was pulsed to each well. The samples were incubated with cells for 72 h or 144 h. The sample-laden medium was then removed from each well. The cells were washed with PBS (1X, pH 7.4) twice. 100 μL of fresh DMEM (no phenol red) and 10 μL of MTT PBS solution (5 mg/ml) were added to each well. After 4 h (37 ^oC, 5% CO_2), 75 μL of medium was removed, and 60 μL DMSO was added into each well to dissolve formazan crystal. The cells were allowed to sit in the incubator (37 ^oC, 5% CO_2) for another 2 h. Finally, the absorbance of each well was

recorded at 540 nm using Biotek Synergy 2 Multi-Mode Microplate Reader (Biotek Instruments, Inc). A calibration curve of absorbance intensity and A549 cell counts was prepared with the same protocol of MTT assay to calculate cell death/proliferation. The calibration curve takes into account any potential solution turbidity.

3.6. Cellular internalization of acid-labile G3NH$_2$-mPEG-nDOX conjugates by A549 cells. 3×10^5 A549 cells/well were seeded in 24-well plates 24 h before the experiment. A 0.5 mL sterile Hanks Balanced Salt Solution (HBSS, 1X, pH 7.4) of free DOX or G3NH$_2$-mPEG-nDOX conjugates (0.1 μM DOX equivalent) was added to each well and then incubated with cells for different lengths of time (0.5, 1, 1.5, 2, 3, 4 and 5 h. n=3 per time point). The cellular internalization was ceased at each time point by replacing sample-laden HBSS with cold blank HBSS. The cells were detached with 0.2 mL 0.25% trypsin-0.53 mM EDTA solution (Life Technologies). The detached cells were pelletized by centrifugation at 350 g. The cell pellet was resuspended in 0.5 mL blank HBSS (4 ^{o}C) and immediately analyzed for DOX fluorescence using flow cytometry (BD LSR II Analyzer, BD Bioscience. San Jose, CA, USA). At least 10,000 events were counted for statistical significance. Median fluorescence intensity (MFI) was plotted as a function of time to evaluate the effect of dendrimer chemistry (PEG density and DOX payload) on cellular internalization.

3.7. Intracellular release and nuclear colocalization of DOX from acid-labile G3NH$_2$-mPEG-nDOX conjugates. 2×10^5 cells were seeded on a cover slide, which was placed in a 24-well plate. After 24 h, a 0.5 mL DMEM (no phenol red) solution of the acid-labile G3NH$_2$-mPEG-nDOX conjugates (4 μM DOX equivalent) was incubated with the cells for 48 h. The sample-containing medium was then thoroughly removed by washing the cells with PBS (1X, pH 7.4) three times.

Nuclei were then stained with Hoechst 33342 (Life Technologies) for 10 min and excess dye was thoroughly washed away with PBS three times. The cells were fixed with 4% paraformaldehyde PBS solution (Sigma-Aldrich) at 4 °C for 20 min and then mounted for imaging. The fixed cells were imaged with Zeiss LSM 780 Confocal Laser Scanning Microscope (Carl Zeiss Microscopy. Oberkrochen, Germany). To evaluate the intracellular release of DOX from acid-labile G3NH_2-mPEG-nDOX conjugates as a function of time (and the free DOX control), the DOX or conjugate-laden medium was incubated with cells for different lengths of time (24, 48, 96 and 144 h, with n=3 per time point). The Pearson's correlation coefficient (PCC) was calculated as a function of time using the Leica LAS AF Lite software (Leica Microsystems. Buffalo Grove, IL, USA). The results were compared with free DOX. Colocalization of the non-labile conjugates was also qualitatively assessed by rendering the 3D confocal images of A549 cell incubated with the G3NH_2-mPEG-nDOXNL conjugates, and stained with nuclear stain.

3.8. Preparation and characterization of the pMDI formulations

3.8.1. Physical stability of acid-labile G3NH_2-mPEG-nDOX conjugate formulation in HFA227 propellant. A predetermined amount of G3NH_2-mPEG-nDOX conjugates and anhydrous ethanol were weighed into pressure proof glass vial (West Pharmaceutical Services. Exton, PA, USA). Subsequently, the glass canister was crimped manually using 63 μL metering valves (Bespak. Norfolk, UK). HFA227 propellant (4 mL) was added to the sealed glass vial with the help of a manual syringe pump (HiP 50-6-15) and a home-made high pressure filler. The resulting formulation was placed in VWR P250D low energy sonication bath (VWR Internationals) for 30 min, which was set to 180 W and 0-5 ^{o}C. The physical stability of the formulations was evaluated by visually monitoring the dispersion as a function of time after sonication.

3.8.2. Particle size measurement. The solvated diameters (SD) of G3NH_2-mPEG-nDOX conjugates were determined using light scattering (LS). Briefly, the aqueous solution of G3NH_2-mPEG-nDOX conjugate was filtered with 0.22 μm syringe filter (VWR Internationals) and then lyophilized. HPFP was also filtered with 0.22 μm syringe filter (VWR Internationals) to remove any impurities in solvent. The purified G3NH_2-mPEG-nDOX conjugate (0.2 mg DOX equivalent) was added to 1 mL HPFP with the help of anhydrous ethanol (0.37 % v/v). The HPFP was added and then sonicated at 0-5 ^{o}C for 30 min. The SD of the conjugate in HPFP was determined using Zetasizer Nano ZS (Malvern Instruments). The average SD and standard deviation (s.d.) were calculated based on at least three measurements.

3.8.3. Aerosol performance of the pMDI formulations. The *in vitro* aerosol characteristics of G3NH_2-mPEG-nDOX pMDI formulations were determined with Andersen Cascade Impactor (CroPharm, Inc. Milford, CT, USA) fitted with a USP induction port. All measurements were operated at a flow rate of 28.3 L/min, 25 ^{o}C and 75% relative humidity.[34] The pMDI formulations were prepared as described above and the canister was loaded into an actuator (orifice 0.22 mm, body length for 14 mL canister. Bespak. Norfolk, UK). Several shots were fired to waste prior to measurement. Subsequently, 10 shots were released into an Anderson Cascade Impactor (ACI) with 10 s interval between shots. The run was promptly stopped 10 s after the last shot. The ACI was dissembled carefully. Actuator, induction port, eight plates and filter membrane were thoroughly rinsed with 10 mL DI H_2O each. The concentration of the G3NH_2-mPEG-nDOX conjugates collected in the aqueous solutions was measured at 490 nm using Cary 50 UV-Vis spectrometer (Agilent Technologies. Santa Clara, CA, USA). The mass of the conjugates deposited on the actuator, induction port, and each plate were calculated relative to an established calibration curve. The following aerosol parameters were calculated: respirable fraction (RF), fine particle

fraction (FPF), mass median aerodynamic diameter (MMAD), geometric standard deviation (GSD) and recovery. The RF is defined as the ratio of mass of particles collected on Stage 0 to filter to the mass of particles released into the ACI. The FPF is defined as the ratio of mass of particles on Stage 3 to filter, to the mass of particles on Induction port to Filter. The MMAD represents the median of the distribution of airborne particle mass with respect to aerodynamic diameter. MMAD is usually reported along with the GSD, which characterizes the variability of the particle size distribution. GSD is defined as the square root of the ratio of 84.13% over 15.87% particle size distribution. Further details on the calculation of MMAD and GSD has been previously reported.[35] The recovery is calculated by dividing collected dose (mass of particles in actuator, induction port, stage 0-7 and filter) by theoretical dose (concentration × volume per puff × puff number).

4. Results and Discussion

4.1. Synthesis and characterization of acid-labile $G3NH_2$-mPEG-nDOX and non-labile $G3NH_2$-mPEG-nDOXNL conjugates. DOX was conjugated to generation 3, amine-terminated PAMAM dendrimers ($G3NH_2$) through an acid-labile cis-aconityl spacer. After forming two amide bonds with DOX and $G3NH_2$, cis-aconityl anhydride has one free carboxyl group (-COOH) left, which can readily catalyze the cleavage of its neighboring intra-molecular amide bond at acidic conditions (i.e. pH < 5), and thus release conjugated DOX – not the pro-drug but DOX itself.[36]

Two synthetic strategies were developed for synthesis of PEGylated PAMAM dendrimers containing different DOX payloads: direct PEGylation for low DOX payloads, and two-step PEGylation for high DOX payloads, as shown in Figure 1.

<< Insert Figure #01 here >>

In the direct PEGylation strategy, cis-aconityl DOX was first conjugated to $G3NH_2$, followed by PEGylation. However, the maximum payload that can be obtained before the conjugate becomes water insoluble was ca. 3.3 DOX. Therefore, an alternative strategy is required in order to prepare $G3NH_2$-DOX conjugates with higher DOX payloads. The way we approached the problem was to first prepare $G3NH_2$ with an initial loading of PEG1000, and only then conjugate the hydrophobic DOX. For a pre-PEGylated $G3NH_2$ with 7PEG1000, we observed that up to 8.8 DOX molecules can be conjugated before the nanoconstruct becomes water insoluble. Based on these observations, it seems that a further increase in DOX payload can be achieved by initially conjugating higher number density of PEG1000. Using this approach, in order to achieve the final / desired PEG density (if greater than 7PEG100), a second round of PEGylation is needed. This two-step PEGylation strategy is a viable approach to achieve both high degree of PEGylation and high DOX payload.

We also attempted another strategy in which high PEGylation preceded DOX conjugation, so as to avoid a two PEGylation strategy. However, only 4.4 DOX can be conjugated to $G3NH_2$-22PEG1000, leading to the failure to achieve high DOX payload. A similar strategy in which PEGylation precedes DOX conjugation has been also reported in an earlier work. High density of peripheral PEG, however, was not attempted (20 PEG out of 64 surface groups) in these reports.[37, 38] However, we will show later that in our work high PEGylation densities are required for the formulation of these nanoconstructs in pMDIs.

In summary, the synthesis of PEGylated PAMAM with low DOX payload (i.e. 3-4 DOX/$G3NH_2$) can be performed independently of the sequence of DOX and PEG conjugation,

while the conjugates with high DOX payload (> 7-9 DOXs/G3NH_2) need to follow the conjugation sequence: 1st PEGylation → DOX conjugation → 2nd PEGylation.

As described for the acid-labile counterparts, the acid-non-labile conjugates with low and high payloads were synthesized via direct PEGylation or two-step PEGylation, with cis-aconityl spacer replaced by succinic linker. The disappearance of free carboxyl group in succinic spacer renders the conjugates stable under both acidic and neutral conditions (G3NH_2-mPEG-nDOXNL).

The acid-labile G3NH_2-mPEG-nDOX and non-labile G3NH_2-mPEG-nDOXNL conjugates were characterized by ^{1}H NMR, MALDI, and ESI. The ESI (m/z) peaks at 700.2016 ([cis-aconityl DOX+H]$^+$), 722.1509 ([cis-aconityl DOX+Na]$^+$), and 738.1769 ([cis-aconityl DOX+K]$^+$) confirm the successful reaction between DOX and cis-aconityl anhydride, while 666.1815 ([succinic DOX+Na]$^+$) and 682.1591 ([succinic DOX+K]$^+$) were assigned to succinic DOX (***Supporting Information***). The ^{1}H NMR peaks at 6.397 ppm (-C*H*=C- of aconityl spacer), 4.025 to 3.936 ppm (-CH_2- in PEG) and characteristic peaks of DOX (see ***Supporting Information***) indicate that DOX was successfully conjugated to dendrimer to form G3NH_2-mPEG-nDOX – Figure 2a. In Figure 2b we show an example of MW change of the conjugates prepared in the two-step approach (G3NH_2-21PEG-7DOX), as monitored by MALDI-TOF. Results for the all other materials are provided in ***Supporting Information***.

<< Insert Figure #02 here >>

The PEG density, DOX payload, and MW of acid-labile G3NH_2-mPEG-nDOX and acid-non-labile G3NH_2-mPEG-nDOXNL conjugates were quantified and are summarized in Table 1 along with their hydrodynamic diameter (HD) and zeta potential (ζ).

<< Insert Table #01 here >>

A series of dendrimers linked with 3 DOX through a pH labile bond or stable bond (control) and varying PEG1000 density were prepared. Another system with 7 DOX was also prepared to compare the effect of DOX loading. The HD is seen to increase upon PEGylation and DOX conjugation, with sizes ranging from 4.0 to 11.3 nm. At low DOX density, the HD is dominated by the PEG density, as all dendrimers with the same PEG density have similar HD, except for G3NH_2-10PEG. G3NH_2-10PEG's small HD may be related to the fact that PEG can more easily form strong bonds with the protonated terminal amine groups of G3NH_2, and thus assume a more collapsed configuration.[39, 40] The addition of 7DOX to the dendrimer with high PEG density seems to have an impact on the overall size, albeit not statistically significant.

We can also observe that the ζ of the nanocarriers decreases from a large positive value for the conjugates with no PEG, to near-neutral at low PEG density or negatively charged at high PEG density – note here that this is the case in spite of the fact that not all surface groups have been modified with PEG, and thus protonated amines are still expected to be present. This effect may be related to the fact that ether oxygen from PEG can strongly interact with the protonated surface amines, thus shielding the surface charge of the nanocarriers.[39, 41] The presence of the extra

carboxyl group of the acid-labile DOX linker also helps decrease the overall charge of the dendrimer, as can be observed by comparing for example $G3NH_2$ (ζ = +18.8 mV) and $G3NH_2$-3DOX (ζ = +6.3 mV). PEGylation also strongly impacts the ζ, with the dendrimers experiencing charge reversal (to negative ζ) at high PEG densities.[31]

Sizes and charges are some of the most relevant parameters in the design of nanocarriers for drug delivery applications, as these properties dictate how the dendrimer nanocarriers interact with the physiological environment, and thus their fate, including bioavailability, pharmacokinetics and pharmacodynamics.[27, 28] The next step in our work was to evaluate the success of the acid-labile DOX conjugation strategy, by determining the release at relevant physiological pHs.

4.2. *In vitro* release of DOX from acid-labile $G3NH_2$-mPEG-nDOX and non-labile $G3NH_2$-mPEG-nDOXNL conjugates at extracellular physiological and lysosomal pH. The DOX released from the acid-labile $G3NH_2$-mPEG-nDOX conjugates and the effect of PEG density on the release of DOX were investigated at pH 7.4 (extracellular physiological pH) and 4.5 (lysosomal pH). The release profiles were compared to that of the acid-non-labile $G3NH_2$-mPEG-nDOXNL conjugates and free DOX, the controls. The results are summarized in Figure 3.

<<Insert Figure #03 here>>

As shown in Figure 3 (b and d), only very small amounts of conjugated DOX are released from the acid-non-labile $G3NH_2$-mPEG-nDOXNL conjugates at either physiological or acidic pH conditions (<4%). In contrast, the release of DOX from $G3NH_2$-mPEG-nDOX is shown to be a

strong function of pH. While small (<9%) amounts of DOX are released from G3NH_2-mPEG-nDOX at pH 7.4, when G3NH_2-mPEG-nDOX is in contact with an acidic medium, > 80-85% DOX is released from the acid-labile conjugates. Based on the released profile of free DOX, we expect the losses of up to ca. 7% of DOX (lack of recovery) due to interactions of DOX with the dialysis bag and to a lesser extent due to photobleaching.

The rate and total amount of DOX released from the acid-labile conjugates is also seen to be a function of the PEGylation density of G3NH_2-mPEG-nDOX. An increase is PEG density is seen to retard the release of DOX. At 50 h, for example, the % release of DOX for G3NH_2-21PEG-3DOX is only 47.6%, while that for G3NH_2-3DOX is 80.3%. The effect of PEGylation can be explained by the increased steric hindrance for proton access to initiate the degradation of the acid-labile linker and also by providing a prolonged diffusion of released hydrophobic DOX out of hydrophilic PEG coating layer.[40]

In summary, the acid-labile PEGylated PAMAM-DOX conjugates showed the potential of being stable at extracellular physiological pH, while a sustained DOX release in conditions mimicking intracellular acidic compartments is achieved. It was also shown that the release of DOX can be further modulated by tailoring the peripheral PEG density. The crucial advantage from acid-labile linker is the potential to decrease the concentration of free DOX in plasma by promoting drug release intracellularly, thus diminishing DOX potential toxicity in general and cardiotoxicity in particular, which may lead to congestive heart failure and death.

4.3. Kill of lung adenocarcinoma cells with acid-labile G3NH_2-mPEG-nDOX and non-labile G3NH_2-mPEG-nDOXNL conjugates. The cytotoxicity of the various DOX conjugates and controls, including free DOX, free dendrimer, and free dendrimer-PEG conjugates was assessed by

MTT assay on A549 cells. The results are summarized in Figure 4. Corresponding IC_{50} values are listed in ***Supporting Information Table S1***.

<<Insert Figure #04 here>>

Neither PAMAM (PEGylated or non-PEGylated) nor acid-non-labile $G3NH_2$-mPEG-nDOXNL showed strong toxicity against A549 cells within the concentration range and incubation time investigated – Figure 4a. Their IC_{50} values could not be detected in the measured range. The toxicity of bare $G3NH_2$ was similar to that of $G3NH_2$-3DOXNL (Figure 4b), demonstrating that the toxicity of the conjugates containing non-labile DOX was mainly induced by the peripheral NH_2 groups of the dendrimers.

In contrast, free DOX and acid-labile conjugates induced significant cell kill on alveolar cancer cells. In Figure 4c it can be observed that the profiles for free DOX and acid-labile DOX are similar, but free DOX is seen to have higher activity at lower concentration. This is to a large extent related to the fact that free DOX can quickly diffuse through the cell bilayer[42, 43] and reach the nucleus, while DOX from the nanocarriers only starts to be released after internalization and traffic to the lysosomes, where the liable bonds will be broken – allowing DOX to finally reach the nucleus.[44, 45] After cleavage, the diffusion of DOX out of lysosome is also a time-consuming process as the base form of weak bases (e.g. DOX) can readily diffuse across internal membrane of lysosome, while their cationic forms (major form of weak bases in lysosomes) diffuse very slowly across the membrane.[46] This effect can be seen to be dominant, as the cell kill profiles for free

DOX and conjugated DOX are seen to be much closer to each other at 144 h post exposure to the dendrimer-DOX conjugates. Another possible reason for the reduced toxicity of conjugated DOX is related to the isomerization during the conjugation of cis-aconityl DOX to dendrimer (cis-aconityl to trans-aconityl DOX),[47] which may result in the failure of original DOX release from the dendrimer conjugates – a pro-drug is released instead. The reduced toxicity of polymer-bound DOX conjugates is consistent with previously published results.[37, 48]

In summary, the conjugation of DOX to dendrimer nanocarriers promotes the control of its release, both temporally and also spatially (intracellular/low pH), and further control can be achieved upon PEGylation. The cell kill curves reflect this temporal controlled release, with DOX toxicity of the conjugates progressively becoming more similar to free DOX profile, as the DOX-dendrimer bonds are slowly broken down upon cellular internalization and transport of the carriers to acidic compartments, and finally diffusion of DOX to reach the nucleus. The impact of PEGylation density on cell kill is small, and becomes negligible at long incubation times, a very favorable result as the interaction of the carriers *in vivo* can be controlled by changing the PEGylation density/surface characteristics of the nanocarriers, [49, 50] and so can its behavior in HFA-propellants used in pMDI formulation, as will be shown later.

4.4. Cellular internalization of acid-labile G3NH_2-mPEG-nDOX conjugates. The kinetics of cellular internalization of the acid-labile G3NH_2-mPEG-nDOX conjugates in A549 cells was evaluated by flow cytometry, by measuring the median fluorescence intensity (MFI) of DOX internalized within the cells as a function of time, for a period of 5 h. The results are summarized in Figure 5.

<<Insert Figure #05 here>>

It can be observed from Figure 5a that the rate and extent of internalization of DOX within 5 h is enhanced upon conjugation to $G3NH_2$. The rate of internalization of DOX in $G3NH_2$-3DOX is 4.7 times greater than free DOX, and the total internalization is statistically different and about 1.6 times as high as free DOX at the end of 5 h. The difference in extent of internalization of free DOX and conjugated DOX is seen to decrease as a function of time. PEGylation is seen to decrease the rate and extent in cellular internalization of conjugated DOX – Figure 5a. It is interesting to note, however, that at the highest PEG density ($G3NH_2$-21PEG-3DOX), the rate and extent of internalization of conjugated DOX is not much different than free DOX, and the means (MFI and rate) are not statistically different at later time points when compared to the same conjugates.

It has been reported that hydrophobic DOX is taken up through passive diffusion and that the diffusion rate is determined by the concentration gradient and interaction with the lipid bilayer.[42, 51] Dendrimer nanocarriers are internalized through different endocytic pathways such as receptor-mediated endocytosis,[44, 52, 53] macropinocytosis,[53] and non-specific, adsorptive endocytosis.[52, 54, 55] The difference in internalization rate of PAMAM-DOX conjugates can be attributed to changes in surface charge. $G3NH_2$-3DOX with a ζ of +6.3 mV is readily adsorbed and quickly saturates the negative plasma membrane.[54] As a consequence, rapid internalization and uptake plateau (1.5 h after incubation) are observed. The uptake plateau may also reveal the equilibrium of internalization and exocytosis of those conjugates. The non-specific, adsorptive endocytosis is faster and less energy-dependent than other endocytic pathways due to its electrostatic interaction.[44] For the PEGylated nanocarriers on the other hand, the ζ becomes less positive as the PEG density

increases (Table 1), reaching negative ζ at the highest density of PEG. The interaction between the negatively charged G3NH_2-mPEG-nDOX and the plasma membrane is thus attenuated, leading to a slowdown in internalization. However, it is important to note that the long-term cytotoxicity studies suggest that high DOX internalization is achieved for all carrier systems, as similar IC_{50} concentrations are observed independent of the PEGylation density.

We also investigated the impact of the DOX loading of the conjugates on the rate and extent of internalization of DOX. The results from Figure 5b show that the rate and extent of internalization of the dendrimer with the higher payload (G3NH_2-21PEG-7DOX) is not statistically different from that for the dendrimer with lower payload (G3NH_2-21PEG-3DOX), indicating that PEGylation dominates the rate and extent of internalization at short times, which is reasonable considering that there are 21PEG and only 7/3DOX per dendrimer, and both impart negative charged characteristics to the dendrimer.

In summary, conjugating DOX to dendrimer nanocarriers enhances their rate and extent of cellular uptake, at least at early times. Cellular internalization of dendrimer-DOX conjugates can be further modulated by PEG density, while the DOX payload on the periphery of the conjugates does not affect uptake when at high PEG densities.

4.5. Intracellular release and colocalization of DOX from acid-labile G3NH_2-mPEG-nDOX conjugates. The intracellular colocalization of free DOX, and DOX from the acid-labile G3NH_2-3DOX and acid-non-labile G3NH_2-3DOXNL conjugates in A549 cells was determined by confocal microscopy. As shown in Figure 6a ("*Overlay*" column), the red fluorescence of DOX in the case of free DOX (first row) and of the DOX from the G3NH_2-DOX conjugate (second row) was highly superposed with the blue staining of the nucleus (Hoechst 33342), revealing significant

colocalization of DOX with the nuclei of A549 cells, the target organelle. Perinuclear colocalization of DOX from $G3NH_2$-DOX indicates that not all DOX had been released at that time. No red fluorescence from DOX was observed in the nuclei for acid-non-labile $G3NH_2$-3DOXNL (third row).

<<Insert Figure #06 here>>

The 3D rendering of the confocal layers for $G3NH_2$-3DOX and $G3NH_2$-3DOXNL shown in Figure 6b further confirms the ability of the conjugates to gain intracellular access, to be trafficked through an acidic pathway, thus releasing the DOX conjugated through the acid labile bond to $G3NH_2$, and finally to co-localize with the nucleus. These results support the cell kill experiments shown in Figure 5. We can also observe that DOX in $G3NH_2$-3DOXNL does not gain access to the nucleus as is not released due to the presence of a pH stable bond between DOX and the dendrimer, and the fact that the dendrimer-DOX conjugate seems to be too large to passively cross the nuclear pores.

These qualitative observations are complemented by quantitative results of the colocalization of DOX (red fluorescent pixels from the confocal slices) with the nucleus (blue fluorescent pixels) as a function of incubation time, upon determination of the Pearson's Correlation Coefficient (PCC) for those fluorescent signals. A PCC = 1 represents complete correlation, while a PCC = 0 represents no correlation.[56] The PCC values for DOX:nucleus for $G3NH_2$-mPEG-nDOX conjugates, and for free DOX (control) are summarized in Figure 7.

<<Insert Figure #07 here>>

The PCC of free DOX is seen to reach 0.87, which represents very high correlation, and this happens at early times - 24 h due to fast colocalization of free DOX within the nucleus. The PCC is seen to level off after ca. 48 h. The PCC for DOX:nucleus in the experiments with the acid-labile $G3NH_2$-mPEG-nDOX conjugates is also seen to be very high at 0.7, indicating strong nuclear colocalization, with a maximum PCC happening at 144 h. However, the maximum PPC for the conjugated DOX is smaller than that seen for free DOX. This lower maximum PCC may be attributed to the isomerization of the conjugates and the fact that there are many potential endocytic pathways for internalization of the conjugates. As cis-aconityl DOX is conjugated to PAMAM dendrimer, cis-aconityl spacer may isomerize to trans-aconityl form.[47] The PAMAM-DOX conjugates with cis-aconityl spacer releases free DOX, whereas the counterparts with trans-aconityl spacer gives rise to aconityl DOX due to the cleavage of amide bond between $G3NH_2$ and linker. The aconityl DOX is not able to get into nucleus due to the loss of the NH_2 group, which is the driving force of DOX to reach the negatively charged DNA.[57] In addition, the conjugates that are internalized by certain endocytic pathways that do not lead to the acidic lysosomes (i.e. caveolae-mediated endocytosis) will have a retarded rate of release for DOX.[58]

The PCC curves are also impacted by PEGylation. They are supported by the cellular internalization (Figure 5) and controlled release (Figure 3) results that show a slowdown in uptake and release as the PEG density increases. The DOX loading is shown not to affect the PPC curves – see curves for $G3NH_2$-21PEG-3DOX and $G3NH_2$-21PEG-7DOX. Finally, it is worth pointing out

that the rate of increase in PCC with time is also slower in the case of the conjugates – compared to free DOX, but it is not clear whether a plateau has been reached at the terminal point of the experiment, which may suggest that higher PCCs for DOX from the conjugates may be achieved.

4.6. Physical stability of the acid-labile G3NH$_2$-mPEG-nDOX conjugates in HFA Propellant. Once the efficacy of the DOX conjugation strategy was assessed *in vitro*, we developed a strategy to formulate dendrimer-DOX conjugates in pMDI formulations for local lung delivery. We are particularly interested in pMDIs due to the many advantages of such portable inhalers, including ease of use and the fact that they are the least expensive OI devices in the market today.[59-61]

We started by investigating the impact of PEGylation and DOX loading on the dispersibility / pseudo-solubilization of the G3NH$_2$-mPEG-nDOX conjugates in HFA277, one of the propellants approved by the FDA for formulation in pMDIs.[62] The stability of the formulations was assessed by visually monitoring the dispersion of G3NH$_2$-mPEG-nDOX conjugates in HFA227 as a function of time after sonication.[63] In order to improve the solubilization/dispersion of the conjugates, a small amount of ethanol (EtOH) cosolvent was added. EtOH is an excipient commonly used in commercial pMDI products, usually at much higher concentrations - up to ca. 15% v/v in commercial formulations [64] However, because the presence of large amounts of EtOH is known to negatively impact aerosol quality in pMDIs,[61, 65, 66] we kept the EtOH concentration to a minimum. The physical stability results of the formulations are summarized in Figure 8.

<<Insert Figure #08 here>>

We can observe that the dispersibility / pseudo-solubilization of the G3NH_2-mPEG-nDOX conjugates is dramatically impacted by the presence of PEG1000. As the PEG1000 density increases, so does the dispersibility of the conjugate, with the conjugate having 21PEG1000 showing excellent dispersibility in HFA227. Our previous *ab initio* calculations and chemical force microscopy results have revealed that ether-containing functionalities (e.g. -CH_2CH_2O-) can be well solvated in HFA propellants as the ether oxygen atom can strongly interact with the dipole of the propellant.[67] The precise conformation of the PEG layer around the dendrimer when the system is dispersed in HFA propellant is still unclear. However, we speculate that some of the segments of the PEG chain may protrude into the propellant, thus acting as a stabilizer as they strongly interact with HFA molecules (HFA-ether complexes),[67] whereas the rest of domains cover the dendrimer surface to form a compact architecture, so as to reduce attractive forces among the dendrimer nanocarriers.[39] Therefore, it is likely that the conjugates in propellant HFA227 take on a core-shell conformation in which PAMAM and DOX consist of the core and PEG chains are situated in the outer shell layer. We also see that at high PEG1000 density the increased payload of HFA-phobic DOX does not affect the dispersibility of the conjugate in the propellant. It is believed that 7 peripheral DOX molecules can be still thoroughly coated by an abundance of grafted PEG chains.

In order to further clarify the nature of the pseudo-solutions/dispersions of the conjugates in HFA, we determined their solvated diameters (SD). We use an HFA that is liquid at ambient conditions and a model liquid propellant — 2H,3H perfluoropentane (HPFP).[68, 69] The results are summarized in Table 2.

<<Insert Table #02 here>>

At low/no PEG1000 density, the $G3NH_2$-mPEG-nDOX conjugates formed large, micron-sized aggregates, which indicates the lack of dispersibility in HFAs. However, upon increasing density of PEG1000 to 21, no micron-sized aggregates can be found. The SDs of the highly PEGylated conjugates were around 30-40 nm. These sizes may represent aggregates of a few conjugates only, or even a single dendrimer conjugate whose SD in HPFP (26 nm for $G3NH_2$-21PEG-3DOX) turns out to be a few times larger than their HD (SD in water – 10 nm $G3NH_2$-21PEG-3DOX) - which are reported in Table 1.

4.7. Aerosol characteristics of pMDI formulations of acid-labile $G3NH_2$-mPEG-nDOX conjugates. While good dispersibility was found for the PEGylated conjugates, the results discussed before do not address the aerosol quality of the resulting formulations. Andersen Cascade Impactor (ACI) is widely used as an *in vitro* lung model to determine drug deposition in the lungs. The correlation of stages to anatomical pulmonary regions are summarized in Figure 9a. Stage 3 and higher represent the lower respiratory tract and deep lung deposition. The effect of PEG density on the aerosol performance of pMDI formulations of $G3NH_2$-mPEG-nDOX conjugates was evaluated and are summarized in Figure 9b and Table 3.

<<Insert Figure #09 here>>

Formulations were prepared at the same conditions as in the physical stability studies discussed earlier - HFA227 propellant at 0.2 mg/mL DOX equivalent and 0.37% v/v EtOH. It can

be observed from Figure 9b that the fraction of DOX (in the conjugate) deposited on stages 3-F increase dramatically at the high PEG density (21PEG1000) compared to no PEG and 9PEG1000. The mass deposition on each stage is summarized in ***Supporting Information Table S2***. The mean mass aerodynamic diameter (MMAD), and the geometric standard deviation (GSD) of the formulations were determined from the ACI results and are summarized in Table 3, along with the respirable fraction (RF) and fine particle fraction (FPF), which represent respirable dose of the formulation and the dose deposited on low respiratory and deep lung area, respectively.

<<Insert Table #03 here>>

While the MMAD for all conjugates fall within the optimum range (5.0-0.5μm), the GSD is much smaller for the highly PEGylated conjugates. More importantly, the RF and FPF for the conjugates with 21PEG1000 (both low and high DOX payload) are much higher than those for $G3NH_2$-3DOX and $G3NH_2$-9PEG-3DOX, the conjugates that showed low dispersibility of the propellant. The RF and FPF for $G3NH_2$-21PEG-3DOX was found to be 82.0% and 78.1%, respectively. For comparison, most of marketed formulations have RF<45%[70-72] of emitted dose and FPF<55%.[34] The RF of the formulation is even higher than HFA-based solution formulations of small molecules (RF: ca. 60-80%) containing soluble excipients.[70, 73] Atomized droplets from the pseudo solution formulation are much smaller than those of poorly dispersed counterparts, which can leads to much smaller particles, which are conducive to deep lung deposition.[65] The recovery for the formulations containing $G3NH_2$-21PEG-3DOX and $G3NH_2$-21PEG-7DOX is much higher than that of the poorly dispersed counterparts. We believe that the loss of the delivered dose of the

formulation containing highly PEGylated conjugates is mainly from small particles with exhalable size range (aerodynamic diameter < 0.5 μm), whereas the strong aggregation of non-PEGylated/low PEGylated conjugates in propellant (big aggregates may not be puffed out) causes the relatively low recovery rate for those nanocarrier systems.

One interesting aspect of this study is the fact that pMDI formulations containing dendrimer conjugates with such small SD – thousand fold smaller than the optimum aerosol diameter - between 0.5 to 5 μm,[74] are capable of generating corresponding aerosols with such exceptional quality.

We propose here a mechanism to explain the results, a schematic diagram of which is shown in Figure 10. In Figure 10a, the pseudo-solution of the G3NH_2-mPEG-nDOX conjugates in HFA propellant is shown – this picture is supported by the SD and physical stability results discussed above. Upon depressing the actuator, droplets containing G3NH_2-mPEG-nDOX and propellant are formed. As the HFA227 propellant evaporates – Figure 10b, the polymer concentration within the droplets increases and it eventually crosses the phase boundary illustrated in Figure 10c – from a single phase to a phase-separated system. Micron-sized particles made of phase-separated G3NH_2-mPEG-nDOX are formed with the appropriate aerosol diameter for deep lung deposition - Figure 10b (iii).

5. Conclusions

In this work we demonstrated the ability of G3NH_2-DOX conjugates to effectively kill A549 cells, an *in vitro* model of alveolar adenocarcinoma. We also developed a novel strategy for the formulation of the conjugates in pMDIs, consisting in forming a pseudo-solution of the

nanocarrier/polymer-drug conjugates in the propellant, which can be achieved upon surface modification of the nanocarrier with a moiety that has high affinity to HFA. DOX was conjugated to $G3NH_2$ through a pH-sensitive bond, which was shown to be a suitable strategy to provide a sustained intracellular release, while being very stable at extracellular physiological conditions. We showed that the release profile of DOX at low pH can be further modulated by the number density of PEG conjugated onto the $G3NH_2$ surface. PEGylation is used to enhance the aqueous solubility of the conjugate at high DOX payloads, and also to promote the formation of the pseudo-solution in the propellant HFA of pMDIs. PEGylation is also observed to decrease the rate and extent of internalization of the dendrimer-DOX conjugates in A549 cells at short times (up to 5h), but the cellular internalization of the conjugates is still greater than that of free DOX even at high PEG density. Nuclear colocalization studies indicate that the dendrimer-DOX conjugates are not only taken up by A549 cells, but the DOX released colocalizes with its target organelle, the nucleus, very efficiently. Interestingly, PEGylation does not affect the ability of the conjugates to kill the adenocarcinoma cells, as all conjugates show similar IC_{50}s to free DOX at long incubation times. Highly stable pseudo-solution of the $G3NH_2$-nDOX conjugates were formed at high PEG densities, as the dipole of HFA can interact very strongly with the ether oxygen of the PEG layer covering the drug-dendrimer conjugate, and thus promote its pseudo-solubilization. The aerosol characteristics of the resulting pMDI formulations were shown to be exceptional, with respirable fractions as high as 82% and fine particle fraction up to 78%. The relevance of the aerosol study goes beyond the formulation of DOX, as other small molecule therapeutics have similar potential to be formulated in pMDIs as dendrimer-drug pseudo solutions using the strategy discussed here.

Fgiures

Figure 1. Synthetic scheme of the PEGylated, generation 3, amine-terminated PAMAM dendrimer ($G3NH_2$) conjugated with DOX. (a) DOX conjugated via an acid-labile linker: $G3NH_2$-mPEG-nDOX; (b) DOX conjugated via a non-labile linker: $G3NH_2$-mPEG-nDOXNL.

Figure 2. Example of (a) ^1H NMR spectra of PEGylated $G3NH_2$ dendrimer with acid-labile DOX conjugates ($G3NH_2$-3DOX and $G3NH_2$-21PEG-7DOX). *Inset*: chemical structure of $G3NH_2$-mPEG-nDOX. Spectral shifts for all compounds are provided in ***Supporting Information S2***, and (b) MALDI spectra of a PEGylated $G3NH_2$ dendrimer with acid-labile DOX conjugates ($G3NH_2$-21PEG-7DOX) and the intermediates synthesized via two-step PEGylation strategy.

Figure 3. *In vitro* release profiles of DOX from the acid-labile ($G3NH_2$-mPEG-nDOX) and non-labile ($G3NH_2$-mPEG-nDOXNL) conjugates at (i) lysosomal pH = 4.5: (a) and (b); (ii) physiological pH = 7.4: (c) and (d), all at 37 ^oC.

Figure 4. Cell kill of (a) $G3NH_2$ and PEGylated dendrimers ($G3NH_2$-mPEG), (b) acid-non-labile conjugates ($G3NH_2$-mPEG-nDOXNL), and (c) acid-labile conjugates ($G3NH_2$-mPEG-nDOX), as determined by the MTT assay after 72 h incubation with A549 cells. (d) Cell kill of acid-labile conjugates ($G3NH_2$-mPEG-nDOX) determined by the MTT assay after 144 h incubation with A549 cells. Free DOX is used as control. Results denote mean ± s.d. (n=8).

Figure 5. (a) Effect of PEGylation on the cellular internalization of the acid-labile ($G3NH_2$-mPEG-nDOX) conjugates in A549 cells as a function of time, as determined by flow cytometry. Results denote mean ± s.d. (n = 3). Statistical significance is calculated with respect to free DOX by one-way ANOVA with Dunnett's test (***$p < 0.001$, **$p < 0.01$, *$p < 0.05$). (b) Effect of DOX payload on the cellular internalization of the acid-labile $G3NH_2$-21PEG-nDOX conjugates in A549 cells as a function of time. Results denote mean ± s.d. (n = 3).

Figure 6. (a) Selected confocal images of A549 cells contacted with free DOX, acid-labile $G3NH_2$-3DOX and acid-non-labile $G3NH_2$-3DOXNL conjugates. (b) Cross section of 3D rendered confocal image of acid-labile $G3NH_2$-3DOX and acid-non-labile $G3NH_2$-3DOXNL conjugates. Image (a) and (b) were obtained 48 h after A549 cells were incubated with the samples. Blue color represents nuclei, red color for DOX, and pink color for DOX co-localized with nuclei.

Figure 7. Pearson's Correlation Coefficient (PCC) of DOX free and from acid-labile G3NH_2-mPEG-nDOX conjugates as a function of incubation time. PCC was determined by confocal microscopy, and calculated based on the colocalization of blue-stained nuclei and red DOX.

Figure 8. Dispersion of acid-labile G3NH_2-mPEG-nDOX in HFA227 propellant as a function of time after sonication. Conditions were: 0.2 mg/mL DOX equivalent; 0.37% anhydrous ethanol (v/v relative to the propellant), at 25^{o}C.

Figure 9. (a) Structure diagram of an Andersen Cascade Impactor (ACI) and correlation of stages in ACI to anatomical regions of the lungs. (b) Aerosol characteristics of the pMDI formulations containing acid-labile conjugates (G3NH_2-mPEG-nDOX) in HFA227 propellant at 0.2 mg/mL DOX equivalent and 0.37% anhydrous ethanol v/v relative to propellant, as determined using ACI at 25 ^{o}C. AC, IP, 0-7 and F denote actuator, induction port, Stage 0-7 and filter, respectively.

Figure 10. Schematic diagram of the proposed mechanism for the formation of the micron size aerosol particles from the nanometer size conjugates. (a) Acid-labile G3NH_2-mPEG-nDOX are solvated as individual particles or nanoaggregates of a few molecules in liquid HFA227 in pMDI at its saturated pressure. (b) As the aerosol forms, the conjugates are (i) initially fully solvated; (ii) as the propellant evaporates, the dendrimer solution phase separates, forming dendrimer nuclei that continue to increase in size to form particles until; (iii) the propellant completely evaporates. (c) Phase separation as the concentration of dendrimer conjugates increases upon evaporation of propellant at ambient pressure.

Acid-labile conjugate **(a)**

Direct PEGylation

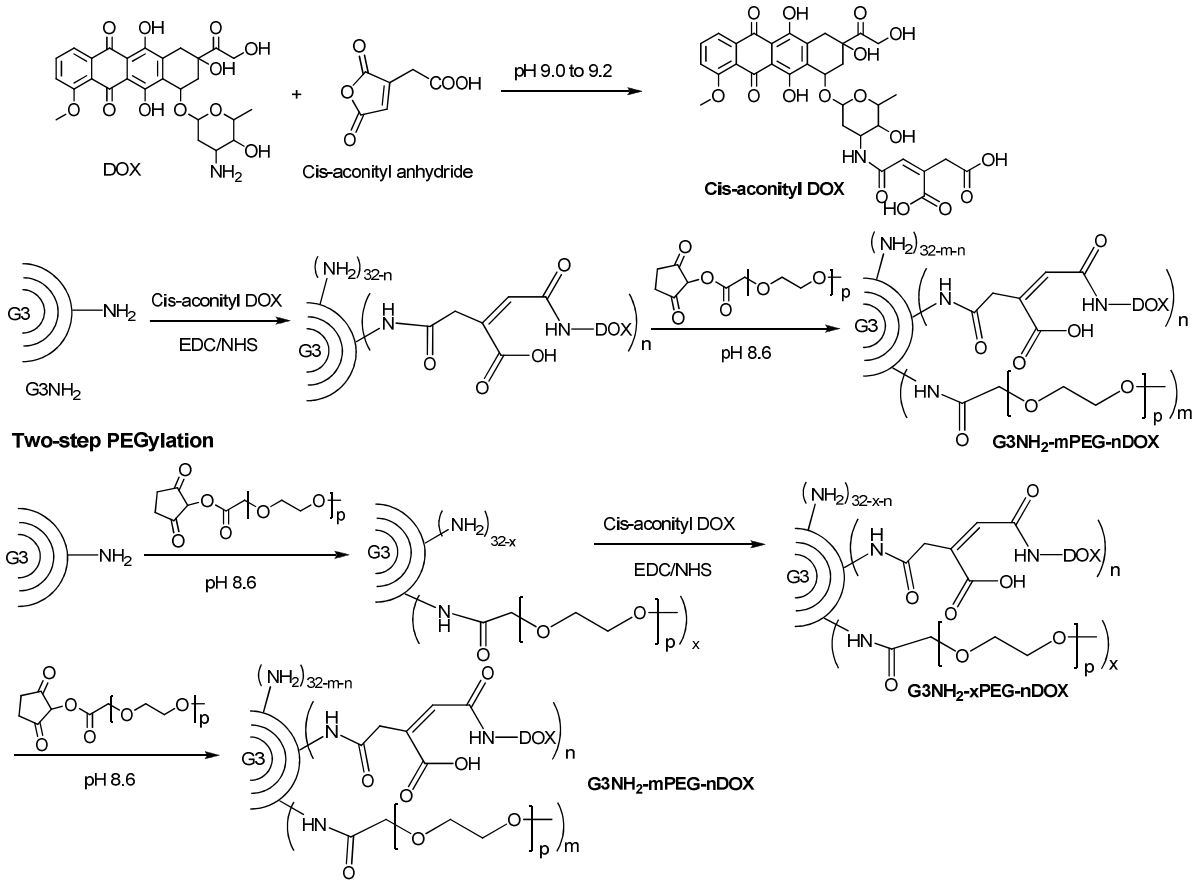

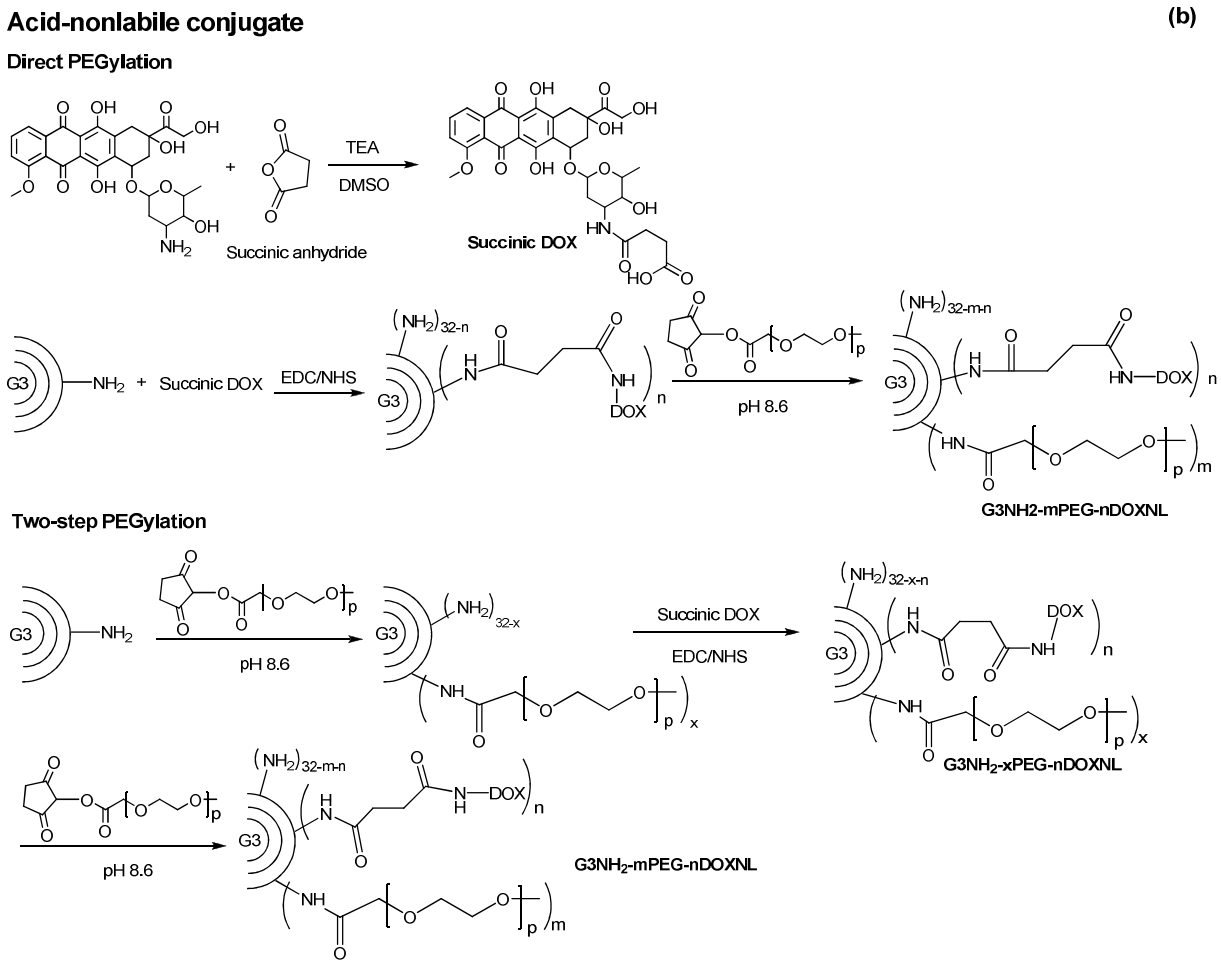
(b)
Acid-nonlabile conjugate
Direct PEGylation
TEA
DMSO
Succinic anhydride
Succinic DOX
EDC/NHS
pH 8.6
G3NH2-mPEG-nDOXNL
Two-step PEGylation
pH 8.6
Succinic DOX
EDC/NHS
G3NH2-xPEG-nDOXNL
pH 8.6
G3NH2-mPEG-nDOXNL

Figure 1.

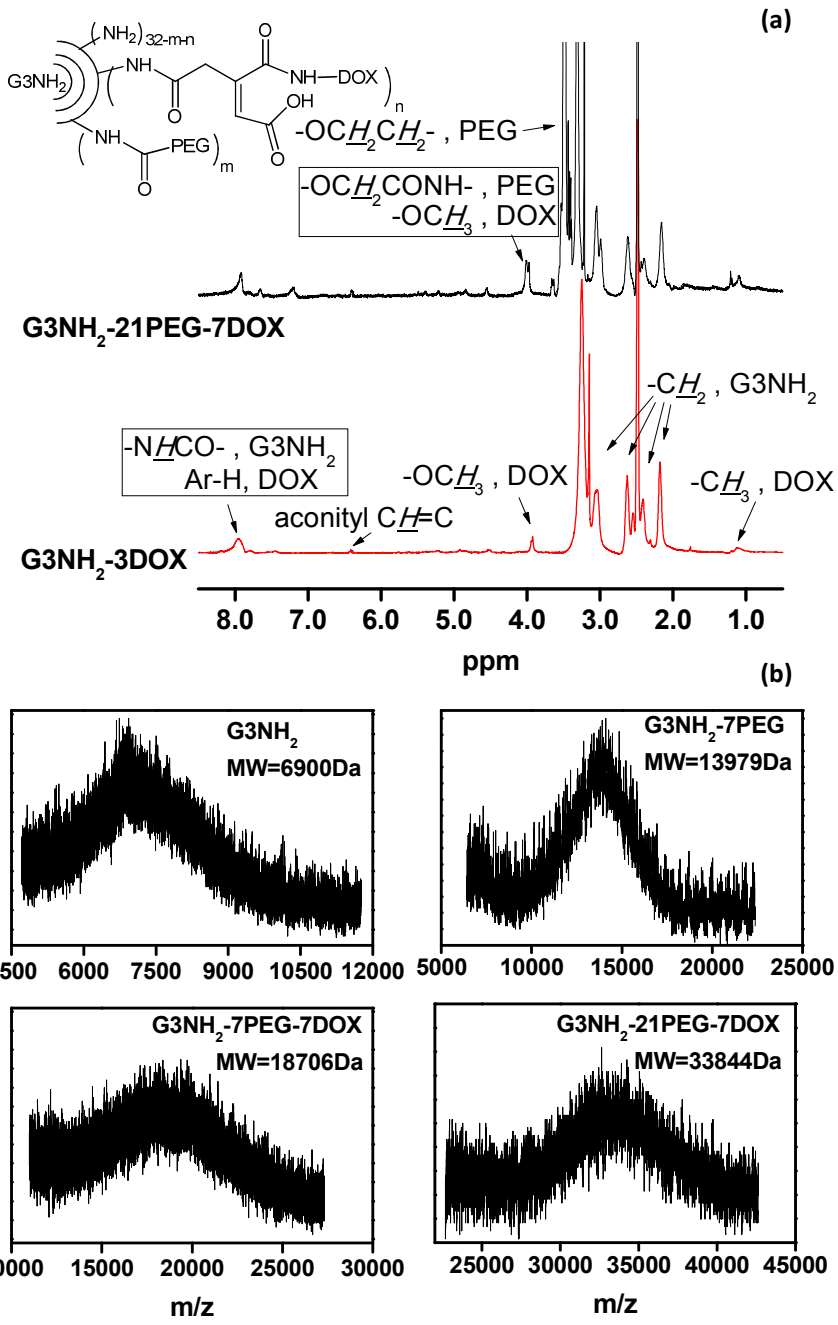
(a)
-OCH2CH2- , PEG
-OCH2CONH- , PEG
-OCH3 , DOX
G3NH2-21PEG-7DOX
-CH2 , G3NH2
-NHCO- , G3NH2
Ar-H, DOX
-OCH3 , DOX
-CH3 , DOX
aconityl CH=C
G3NH2-3DOX
8.0 7.0 6.0 5.0 4.0 3.0 2.0 1.0
ppm
(b)
G3NH2
MW=6900Da
G3NH2-7PEG
MW=13979Da
G3NH2-7PEG-7DOX
MW=18706Da
G3NH2-21PEG-7DOX
MW=33844Da
m/z
m/z

Figure 2.

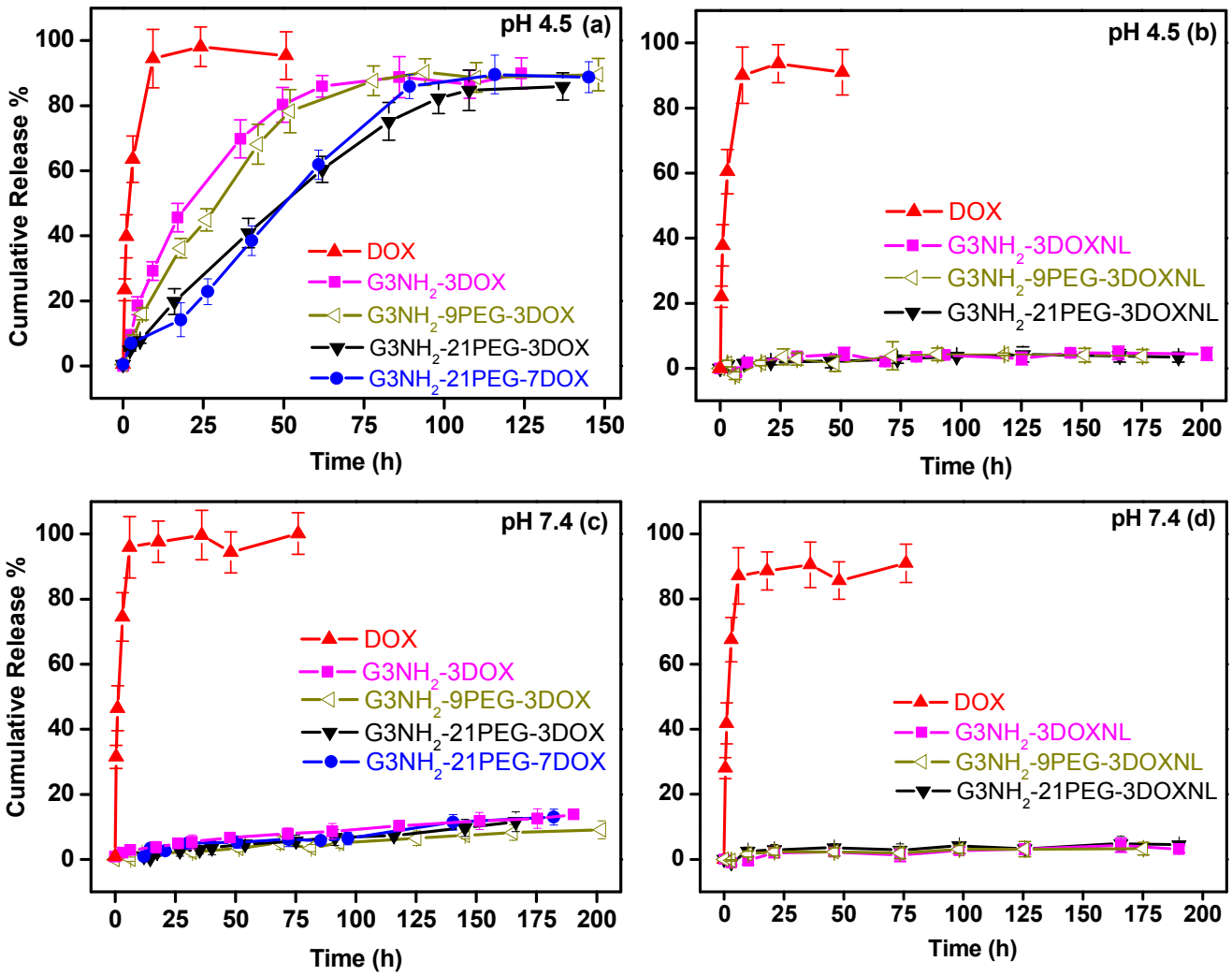
pH 4.5 (a)
pH 4.5 (b)
pH 7.4 (c)
pH 7.4 (d)
Cumulative Release %
Time (h)
DOX
G3NH2-3DOX
G3NH2-9PEG-3DOX
G3NH2-21PEG-3DOX
G3NH2-21PEG-7DOX
G3NH2-3DOXNL
G3NH2-9PEG-3DOXNL
G3NH2-21PEG-3DOXNL

Figure 3.

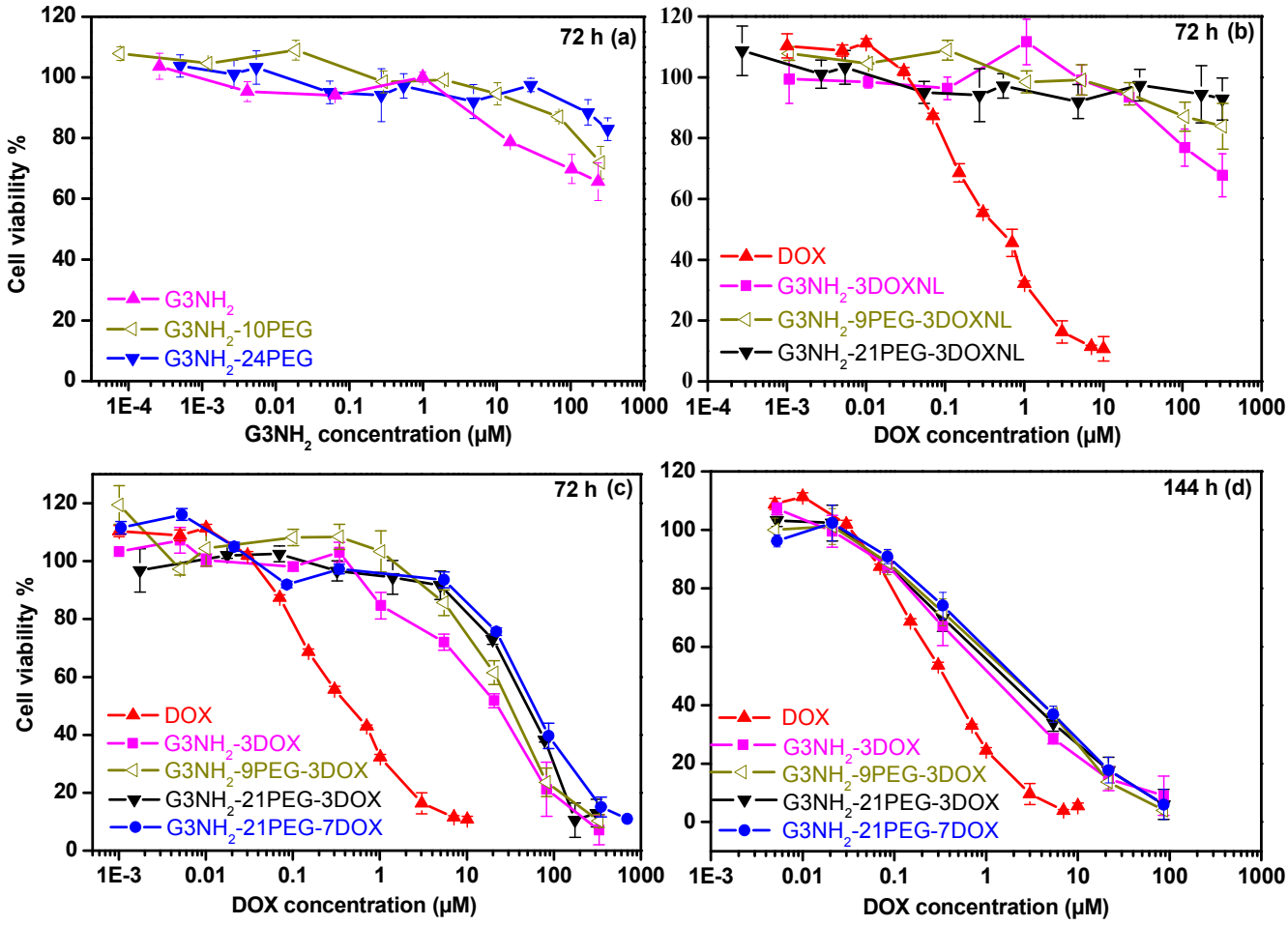
72 h (a)
Cell viability %
G3NH2
G3NH2-10PEG
G3NH2-24PEG
G3NH2 concentration (μM)
72 h (b)
DOX
G3NH2-3DOXNL
G3NH2-9PEG-3DOXNL
G3NH2-21PEG-3DOXNL
DOX concentration (μM)
72 h (c)
Cell viability %
DOX
G3NH2-3DOX
G3NH2-9PEG-3DOX
G3NH2-21PEG-3DOX
G3NH2-21PEG-7DOX
DOX concentration (μM)
144 h (d)
DOX
G3NH2-3DOX
G3NH2-9PEG-3DOX
G3NH2-21PEG-3DOX
G3NH2-21PEG-7DOX
DOX concentration (μM)

Figure 4.

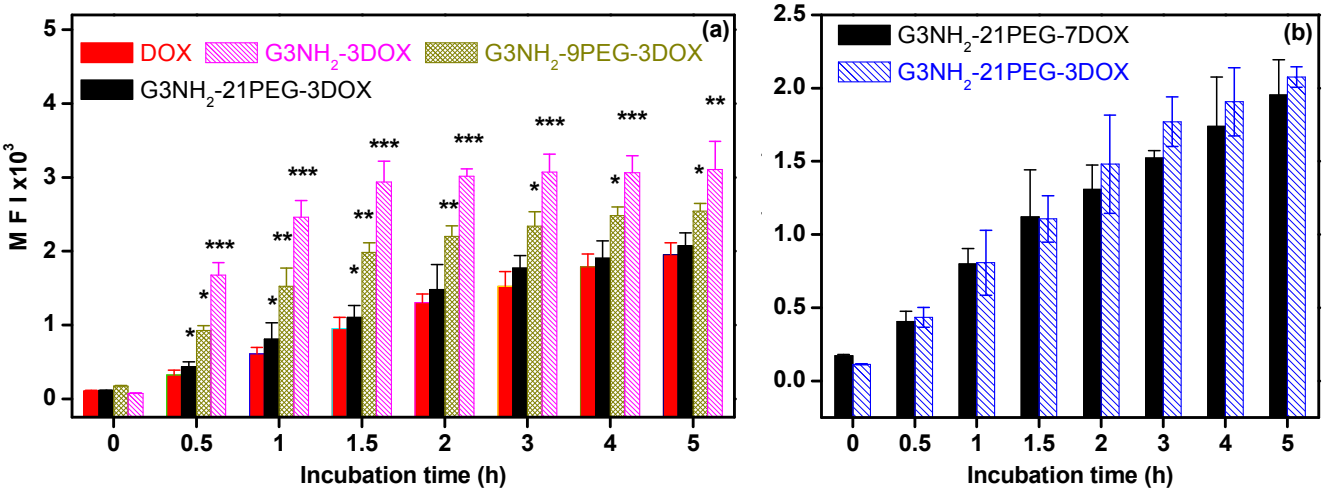
(a)
DOX
G3NH2-3DOX
G3NH2-9PEG-3DOX
G3NH2-21PEG-3DOX
M F I x10^3
Incubation time (h)
(b)
G3NH2-21PEG-7DOX
G3NH2-21PEG-3DOX
Incubation time (h)

Figure 5.

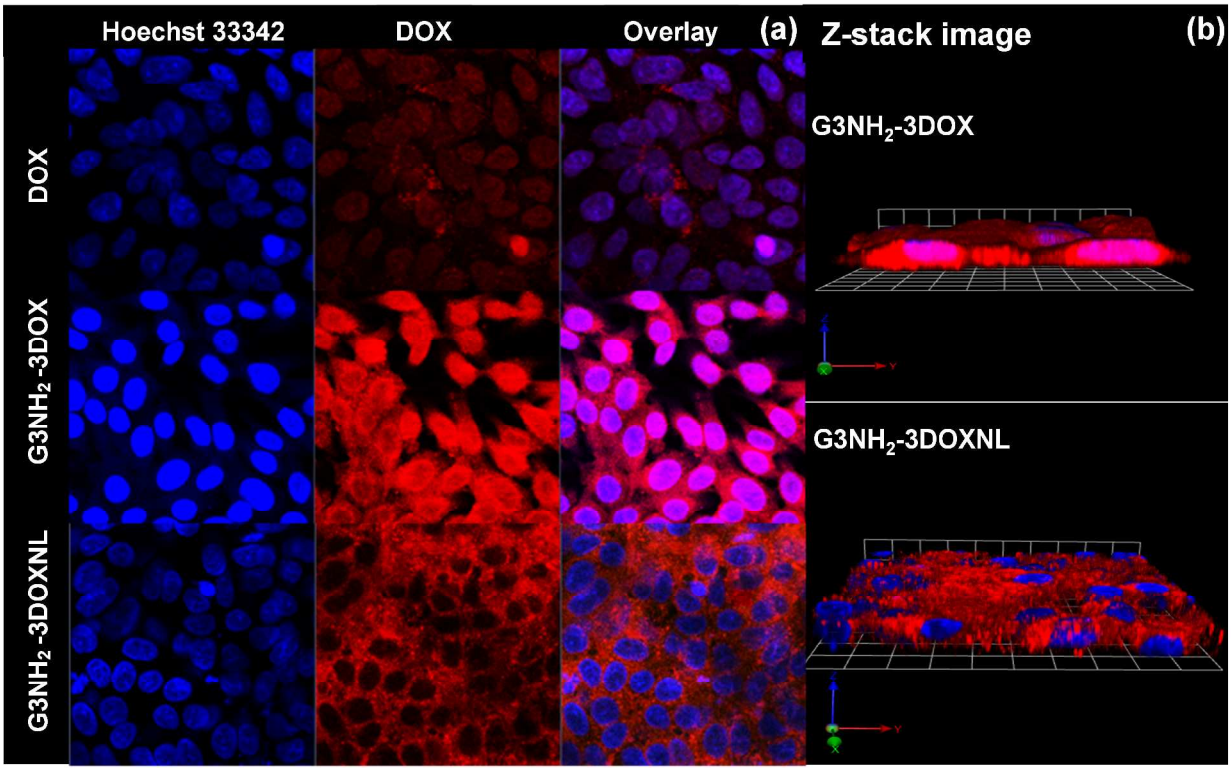
Hoechst 33342
DOX
Overlay
(a)
Z-stack image
(b)
DOX
G3NH2 -3DOX
G3NH2 -3DOXNL
G3NH2-3DOX
G3NH2-3DOXNL

Figure 6.

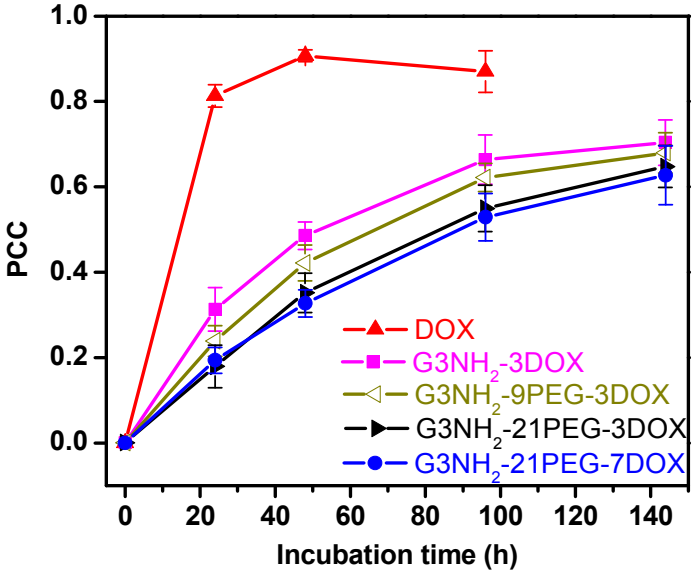
1.0
0.8
0.6
0.4
0.2
0.0
PCC
0
20
40
60
80
100
120
140
Incubation time (h)
DOX
G3NH2-3DOX
G3NH2-9PEG-3DOX
G3NH2-21PEG-3DOX
G3NH2-21PEG-7DOX

Figure 7.

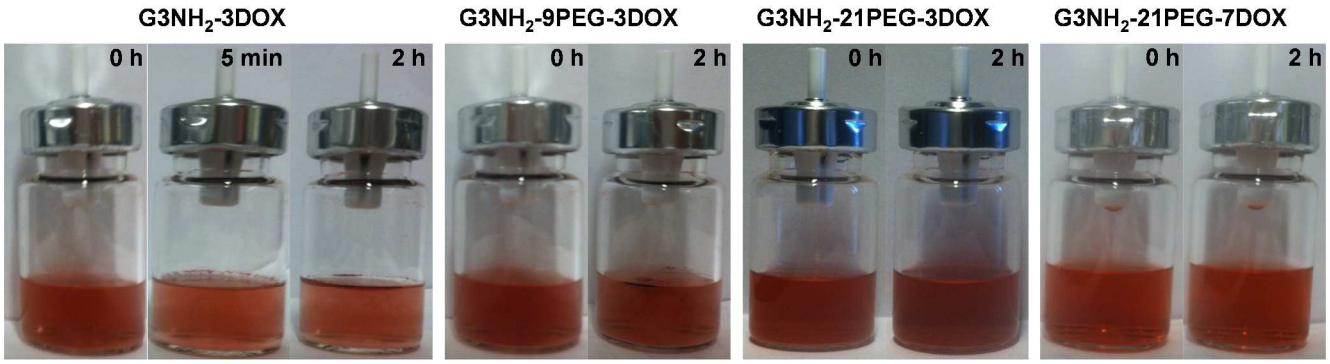
G3NH2-3DOX
G3NH2-9PEG-3DOX
G3NH2-21PEG-3DOX
G3NH2-21PEG-7DOX
0 h
5 min
2 h
0 h
2 h
0 h
2 h
0 h
2 h

Figure 8.

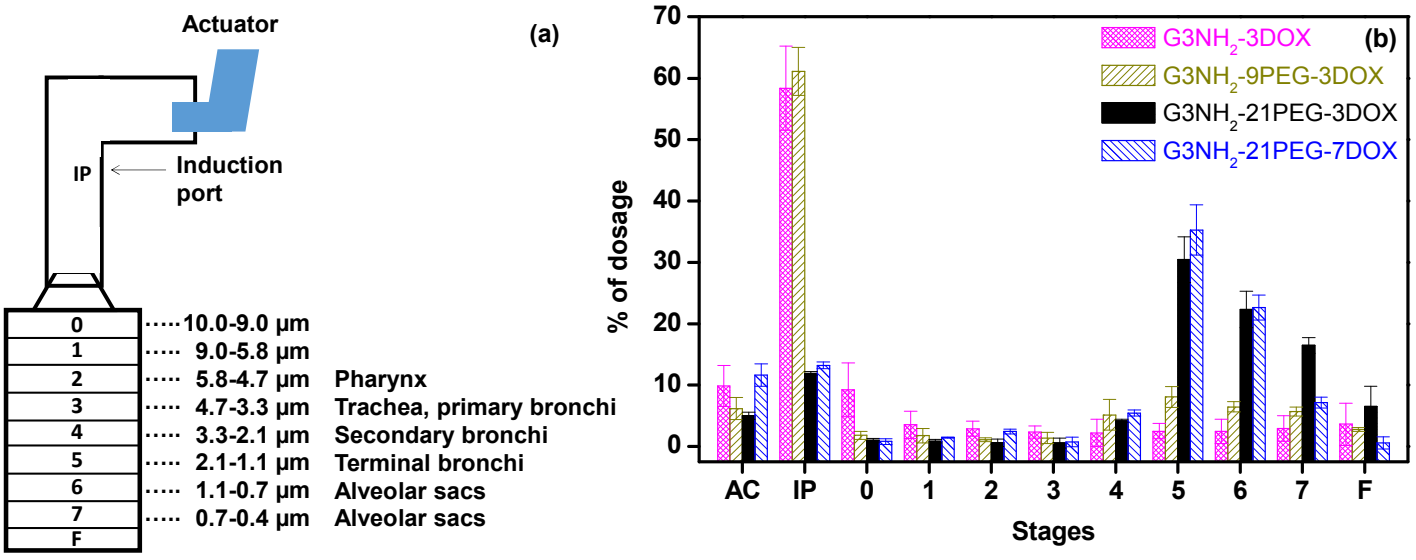
Actuator
IP
Induction port
(a)
0
1
2
3
4
5
6
7
F
10.0-9.0 μm
9.0-5.8 μm
5.8-4.7 μm
4.7-3.3 μm
3.3-2.1 μm
2.1-1.1 μm
1.1-0.7 μm
0.7-0.4 μm
Pharynx
Trachea, primary bronchi
Secondary bronchi
Terminal bronchi
Alveolar sacs
Alveolar sacs
(b)
G3NH2-3DOX
G3NH2-9PEG-3DOX
G3NH2-21PEG-3DOX
G3NH2-21PEG-7DOX
% of dosage
0
10
20
30
40
50
60
70
AC
IP
0
1
2
3
4
5
6
7
F
Stages

Figure 9.

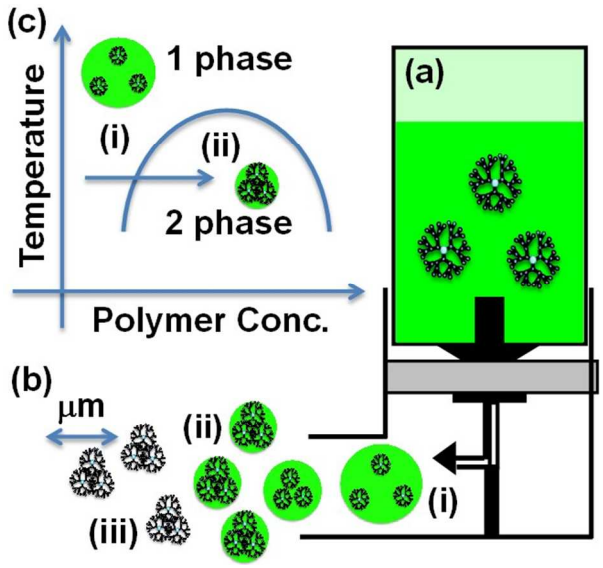

Figure 10.

Tables

Table 1. Molecular weight (MW), number of PEG1000 grafts (*m*), number of doxorubicin (DOX) conjugates (*n*), hydrodynamic diameter (HD), and zeta potential (ζ) of the PEGylated, generation 3, amine-terminated PAMAM dendrimer ($G3NH_2$) conjugates. DOX conjugated via an acid-labile linker: $G3NH_2$-mPEG-nDOX; DOX conjugated via a non-labile linker: $G3NH_2$-mPEG-nDOXNL. Results obtained by ^{1}H NMR, MALDI, and light scattering (LS) at 25°C. s.d. = standard deviation.

Conjugate	MW	m_{PEG}		n_{DOX}		HD ± s.d. (nm)	ζ ± s.d. (mV)
		^{1}H NMR	MALDI	^{1}H NMR	MALDI		
$G3NH_2$	6900	-	-	-	-	3.8 ± 1.3	+18.8 ± 5.0
$G3NH_2$-10PEG	16436	9.8	9.0	-	-	4.6 ± 1.4	+3.0 ± 4.1
$G3NH_2$-24PEG	32419	24.5	24.1	-	-	8.8 ± 3.7	-2.1 ± 5.4
$G3NH_2$-3DOXNL	8915	-	-	3.4	3.1	4.3 ± 1.5	+14.2 ± 3.3
$G3NH_2$-9PEG-3DOXNL	18975	9.4	9.5	2.6	3.1	7.7 ± 3.5	+2.0 ± 3.6
$G3NH_2$-21PEG-3DOXNL	31077	20.7	21.0	3.1	3.1	8.9 ± 4.2	-3.7 ± 4.9
$G3NH_2$-3DOX	9133	-	-	3.5	3.3	4.0 ± 2.3	+6.3 ± 3.5
$G3NH_2$-9PEG-3DOX	19130	8.8	7.5	2.9	3.3	6.9 ± 3.2	-2.1 ± 4.3
$G3NH_2$-21PEG-3DOX	31220	21.4	20.9	3.1	3.3	9.6 ± 4.9	-6.6 ± 2.7
$G3NH_2$-21PEG-7DOX	33844	21.1	20.5	7.4	6.9	11.3 ± 4.3	-10.5 ± 6.1

Table 2. Solvated diameter (SD) and polydispersity index (PDI) of the PEGylated (*m*), generation 3, amine-terminated PAMAM dendrimer ($G3NH_2$) conjugates with DOX measured in the model propellant HPFP. DOX conjugated via an acid-labile linker ($G3NH_2$-mPEG-nDOX). Results determined by light scattering (LS) at 25°C and 0.2 mg/mL DOX equivalent. n.p. = not present; % in parenthesis = volume fraction within that diameter range.

Conjugate	SD ± s.d.		PDI
	Peak A	Peak B	
$G3NH_2$-3DOX	0.5 ± 0.1 μm (13.3%)	6.1 ± 2.8 μm	0.732
$G3NH_2$-9PEG-3DOX	0.7 ± 0.1 μm (15.1%)	4.2 ± 1.2 μm	0.663
$G3NH_2$-21PEG-3DOX	26.1 ± 7.8 nm (100%)	n.p.	0.108
$G3NH_2$-21PEG-7DOX	38.3 ± 11.6 nm (100%)	n.p.	0.125

Table 3. Median mass aerodynamic diameter (MMAD), geometric standard deviation (GSD), respirable fraction (RF), fine particle fraction (FPF) and recovery (%) of the pMDI formulation containing the PEGylated (*m*), generation 3, amine-terminated PAMAM dendrimer ($G3NH_2$) dendrimers conjugated with DOX via an acid-labile linker ($G3NH_2$-mPEG-nDOX). Aerosol results determined using the Andersen Cascade Impactor (ACI), at 25°C. Formulation containing 0.2 mg of DOX equivalent per mL of propellant and anhydrous ethanol at 0.37% v/v relative to the propellant. Propellant is HFA227.

Conjugates	MMAD (µm)	GSD (µm)	RF (%)	FPF (%)	Recovery (%)
$G3NH_2$-3DOX	4.5 ± 1.9	6.6 ± 2.4	31.8 ± 3.9	16.1 ± 1.8	65.7 ± 6.4
$G3NH_2$-9PEG-3DOX	3.3 ± 0.8	3.9 ± 1.4	33.1 ± 5.9	29.7 ± 3.7	69.2 ± 7.1
$G3NH_2$-21PEG-3DOX	1.2 ± 0.1	1.9 ± 0.1	82.0 ± 4.8	78.1 ± 4.3	86.9 ± 4.7
$G3NH_2$-21PEG-7DOX	1.2 ± 0.1	1.6 ± 0.1	75.4 ± 3.0	70.8 ± 5.4	84.6 ± 5.5

ASSOCIATED CONTENT

Supporting Information. Description of synthesis and characterization of the acid-labile and acid-non-labile PEGylated dendrimer-DOX conjugates/structures including ^{1}H NMR, ESI, MALDI-TOF and LS. The IC_{50} of free DOX and various PEGylated dendrimer-DOX conjugates and aerosol mass deposition in ACI of pMDI formulation containing dendrimer-DOX conjugates are also provided. This material is available free of charge via the Internet at http://pubs.acs.org.

AUTHOR INFORMACTION

Corresponding Author

Sandro R. P. da Rocha
Department of Pharmaceutics &
Department of Chemical and Life Science Engineering
Virginia Commonwealth University
Smith Building, 4th Floor, Room 450A
410 North 12th Street
P.O.Box 980533
Richmond, Virginia 23298-0533
Phone: (804) 828-0985 / Fax: (804) 828-8359
Email: srdarocha@vcu.edu

Notes

The authors declare no competing financial interests.

ABBREVIATIONS

PAMAM: poly(amidoamine); G3NH2: Generation 3 amine-terminated PAMAM dendrimer; PEG: polyethylene glycol; DOX: doxorubicin; SA: succinic anhydride; CA: cis-aconitic anhydride; SAD

succinic doxorubicin; CAD: cis-aconitic doxorubicin.$G3NH_2$-mPEG-nDOXNL: $G3NH_2$ dendrimer with m PEG and n SAD on the surface; $G3NH_2$-mPEG-nDOX: $G3NH_2$ dendrimer with m PEG and n CAD on the surface; EDC: N-(3-dimethylaminopropyl)-N'-ethylcarbodiimide; NHS: N-Hydroxysuccinimide; TEA: triethylamine; SA: succinic anhydride; CA: cis-aconitic anhydride; SAD succinic doxorubicin; CAD: cis-aconitic doxorubicin. p-TSA: p-toluenesulfonic acid monohydrate; DMSO: dimethylsulfoxide; DMF: dimethylformamide; 2, 5-DHB: 2, 5-dihydroxybenzoic acid; MWCO: Molecular Weight Cut Off; DI water: deionized water; DMEM: Dulbecco's Modified Eagle Medium; HBSS: Hank's Balanced Salt Solution; PBS: phosphate buffer saline; ^{1}H NMR: proton nuclear magnetic resonance; ESI: electrospray ionization; MALDI: mass-assisted laser desorption/ionization; LS: light scattering; MW: molecular weight; HD: hydrodynamic diameter; MFI: median fluorescence intensity; PCC: Pearson's correlation coefficient; SD: solvation diameter; HFA: hydrofluoroalkane; HPFP: 2H, 3H perfluoropentane; RF: respirable fraction; FPF: fine particle fraction; MMAD: mass median aerodynamic diameter; GSD: geometric standard deviation; IP: induction port; ACI: Andersen Cascade Impactor.

ACKONWLEDGEMENTS

We would like to acknowledge financial support from National Science Foundation (NSF-CBET grant no.0933144 and NSF-DMR grant no. 1508363) and the NanoIncubator at Wayne State University (WSU). We would also like to thank Dr. Jessica Back and Mr. Eric Van Buren (Microscopy, Imaging and Cytometry Resources Core) for useful discussions regarding flow cytometry analysis. The MICR Core is supported, in part, by NIH CenterGrant P30CA022453 to the Karmanos Cancer Institute and the Perinatology Research Branch of the National Institutes of Child Health and Development, both at WSU.

For Table of Contents Use Only

Poly(amidoamine) Dendrimer-Doxorubicin Conjugates: *In vitro* characteristics and Pseudo-Solution Formulation in Pressurized Metered-Dose Inhalers

Qian Zhong and Sandro R. P. da Rocha

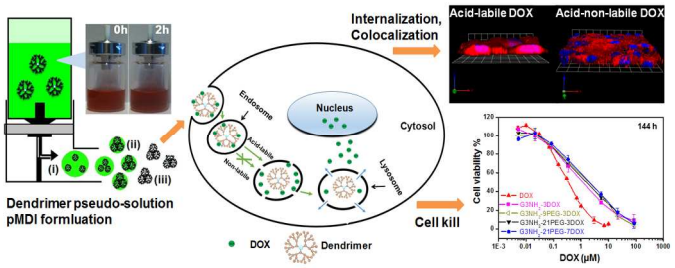

REFERENCES

1. Siegel, R.; Naishadham, D.; Jemal, A. Cancer statistics, 2013. *Ca-Cancer J. Clin.* **2013,** *63*, (1), 11-30.
2. Murphy, S. L.; Xu, J.; Kochanek, K. D. Deaths: final data for 2010. *Natl. Vital. Stat. Rep.* **2013,** *61*, (4), 1-118.
3. American Cancer Society *Cancer Facts & Figures 2014 (Report)*; 2014.
4. Centers for Disease Control and Prevention. Lung Cancer. http://www.cdc.gov/cancer/lung/basic_info/index.htm (March 15),
5. Siegel, R.; Naishadham, D.; Jemal, A. Cancer statistics, 2012. *Ca-Cancer J. Clin.* **2012,** *62*, (1), 10-29.
6. Chojniak, R.; Yu, L.; Younes, R. Response to chemotherapy in patients with lung metastases: how many nodules should be measured? *Cancer Imaging* **2006,** *6*, (1), 107.
7. Pilkington, G.; Boland, A.; Brown, T.; Oyee, J.; Bagust, A.; Dickson, R. A systematic review of the clinical effectiveness of first-line chemotherapy for adult patients with locally advanced or metastatic non-small cell lung cancer. *Thorax* **2015**, thoraxjnl-2014-205914.
8. Otterson, G. A.; Villalona-Calero, M. A.; Sharma, S.; Kris, M. G.; Imondi, A.; Gerber, M.; White, D. A.; Ratain, M. J.; Schiller, J. H.; Sandler, A. Phase I study of inhaled Doxorubicin for patients with metastatic tumors to the lungs. *Clin. Cancer Res.* **2007,** *13*, (4), 1246-1252.
9. Lee, W.-H.; Loo, C.-Y.; Ong, H.-X.; Traini, D.; Young, P. M.; Rohanizadeh, R. Synthesis and Characterization of Inhalable Flavonoid Nanoparticle for Lung Cancer Cell Targeting. **2015**.
10. Sharma, S.; White, D.; Imondi, A. R.; Placke, M. E.; Vail, D. M.; Kris, M. G. Development of inhalational agents for oncologic use. *J. Clin. Oncol.* **2001,** *19*, (6), 1839-1847.
11. Cheng, C.; Haouala, A.; Krueger, T.; Mithieux, F.; Perentes, J. Y.; Peters, S.; Decosterd, L. A.; Ris, H.-B. Drug uptake in a rodent sarcoma model after intravenous injection or isolated lung perfusion of free/liposomal doxorubicin. *Interact. Cardiovasc. Thorac. Surg.* **2009,** *8*, (6), 635-638.
12. Broxterman, H. J.; Versantvoort, C. H.; Linn, S. C., Multidrug resistance in lung cancer. In *Lung Cancer*, Springer: 1995; pp 193-222.
13. Kelland, L. The resurgence of platinum-based cancer chemotherapy. *Nat. Rev. Cancer* **2007,** *7*, (8), 573-584.
14. Otterson, G. A.; Villalona-Calero, M. A.; Hicks, W.; Pan, X.; Ellerton, J. A.; Gettinger, S. N.; Murren, J. R. Phase I/II Study of inhaled doxorubicin combined with platinum-based therapy for advanced non–small cell lung cancer. *Clin. Cancer Res.* **2010,** *16*, (8), 2466-2473.
15. Wieland, S.; Mita, A.; Piantadosi, S.; Natale, R.; Levitt, D. In *Phase 2 Study of Aldoxorubicin Versus Topetecan for Relapsed/Refractory Small Cell Lung Cancer*, Annals of Oncology, 2014; OXFORD UNIV PRESS GREAT CLARENDON ST, OXFORD OX2 6DP, ENGLAND.
16. Minotti, G.; Menna, P.; Salvatorelli, E.; Cairo, G.; Gianni, L. Anthracyclines: molecular advances and pharmacologic developments in antitumor activity and cardiotoxicity. *Pharmacol. Rev.* **2004,** *56*, (2), 185-229.
17. Carvalho, F. S.; Burgeiro, A.; Garcia, R.; Moreno, A. J.; Carvalho, R. A.; Oliveira, P. J. Doxorubicin - Induced Cardiotoxicity: From Bioenergetic Failure and Cell Death to Cardiomyopathy. *Med. Res. Rev.* **2014,** *34*, (1), 106-135.
18. Bristow, M.; Billingham, M.; Mason, J.; Daniels, J. Clinical spectrum of anthracycline antibiotic cardiotoxicity. *Annu. Rev. Biomed. Eng.* **1978,** *62*, (6), 873-879.

19. Villani, F.; Beretta, G.; Guindani, A. Evaluation of early doxorubicin-induced cardiotoxicity by means of systolic time intervals. *Cancer Chemother. Pharmacol.* **1979,** *3*, (4), 249-251.
20. Chatterjee, K.; Zhang, J.; Honbo, N.; Karliner, J. S. Doxorubicin cardiomyopathy. *Cardiology* **2009,** *115*, (2), 155-162.
21. Carvalho, F. S.; Burgeiro, A.; Garcia, R.; Moreno, A. J.; Carvalho, R. A.; Oliveira, P. J. Doxorubicin-Induced Cardiotoxicity: From Bioenergetic Failure and Cell Death to Cardiomyopathy. *Med. Res. Rev.* **2014,** *34*, (1), 106-135.
22. Wang, X.; Li, S.; Shi, Y.; Chuan, X.; Li, J.; Zhong, T.; Zhang, H.; Dai, W.; He, B.; Zhang, Q. The development of site-specific drug delivery nanocarriers based on receptor mediation. *J. Controlled Release* **2014,** *193*, 139-153.
23. Gautier, J.; Allard-Vannier, E.; Munnier, E.; Soucé, M.; Chourpa, I. Recent advances in theranostic nanocarriers of doxorubicin based on iron oxide and gold nanoparticles. *J. Controlled Release* **2013,** *169*, (1), 48-61.
24. Albanese, A.; Tang, P. S.; Chan, W. C. The effect of nanoparticle size, shape, and surface chemistry on biological systems. *Annu. Rev. Biomed. Eng.* **2012,** *14*, 1-16.
25. Bosselmann, S.; Williams III, R. O. Has nanotechnology led to improved therapeutic outcomes? *Drug Dev. Ind. Pharm.* **2012,** *38*, (2), 158-170.
26. Tomalia, D. A.; Naylor, A. M.; Goddard, W. A. Starburst dendrimers: molecular‐level control of size, shape, surface chemistry, topology, and flexibility from atoms to macroscopic matter. *Angew. Chem., Int. Ed. Engl.* **1990,** *29*, (2), 138-175.
27. Cheng, Y.; Xu, T. The effect of dendrimers on the pharmacodynamic and pharmacokinetic behaviors of non-covalently or covalently attached drugs. *Eur. J. Med. Chem.* **2008,** *43*, (11), 2291-2297.
28. Kaminskas, L. M.; Boyd, B. J.; Porter, C. J. Dendrimer pharmacokinetics: the effect of size, structure and surface characteristics on ADME properties. *Nanomedicine* **2011,** *6*, (6), 1063-1084.
29. Menjoge, A. R.; Kannan, R. M.; Tomalia, D. A. Dendrimer-based drug and imaging conjugates: design considerations for nanomedical applications. *Drug Discovery Today* **2010,** *15*, (5), 171-185.
30. Nigavekar, S. S.; Sung, L. Y.; Llanes, M.; El-Jawahri, A.; Lawrence, T. S.; Becker, C. W.; Balogh, L.; Khan, M. K. 3H dendrimer nanoparticle organ/tumor distribution. *Pharm. Res.* **2004,** *21*, (3), 476-483.
31. Bharatwaj, B.; Mohammad, A. K.; Dimovski, R.; Cassio, F. L.; Bazito, R. C.; Conti, D.; Fu, Q.; Reineke, J.; da Rocha, S. R. Dendrimer Nanocarriers for Transport Modulation Across Models of the Pulmonary Epithelium. *Mol. Pharmaceutics* **2015,** *12*, (3), 826-838.
32. Tomlinson, R.; Heller, J.; Brocchini, S.; Duncan, R. Polyacetal-doxorubicin conjugates designed for pH-dependent degradation. *Bioconjugate Chem.* **2003,** *14*, (6), 1096-1106.
33. Shen, W.-C.; Ryser, H. J.-P. cis-Aconityl spacer between daunomycin and macromolecular carriers: a model of pH-sensitive linkage releasing drug from a lysosomotropic conjugate. *Biochem. Biophys. Res. Commun.* **1981,** *102*, (3), 1048-1054.
34. Conti, D. S.; Brewer, D.; Grashik, J.; Avasarala, S.; da Rocha, S. R. Poly (amidoamine) dendrimer nanocarriers and their aerosol formulations for siRNA delivery to the lung epithelium. *Mol. Pharmaceutics* **2014,** *11*, (6), 1808-1822.
35. Wu, L.; Al-Haydari, M.; da Rocha, S. R. Novel propellant-driven inhalation formulations: engineering polar drug particles with surface-trapped hydrofluoroalkane-philes. *Eur. J. Pharm. Sci.* **2008,** *33*, (2), 146-158.

36. Bender, M. L. General Acid-Base Catalysis in the Intramolecular Hydrolysis of Phthalamic Acid. *J. Am. Chem. Soc.* **1957,** *79*, (5), 1258-1259.
37. Zhu, S.; Hong, M.; Tang, G.; Qian, L.; Lin, J.; Jiang, Y.; Pei, Y. Partly PEGylated polyamidoamine dendrimer for tumor-selective targeting of doxorubicin: the effects of PEGylation degree and drug conjugation style. *Biomaterials* **2010,** *31*, (6), 1360-1371.
38. Zhu, S.; Hong, M.; Zhang, L.; Tang, G.; Jiang, Y.; Pei, Y. PEGylated PAMAM dendrimer-doxorubicin conjugates: in vitro evaluation and in vivo tumor accumulation. *Pharm. Res.* **2010,** *27*, (1), 161-174.
39. Yang, L.; da Rocha, S. R. P. PEGylated, NH2-Terminated PAMAM Dendrimers: A Microscopic View from Atomistic Computer Simulations. *Mol. Pharmaceutics* **2014,** *11*, (5), 1459-1470.
40. Riechers, S.; Zhong, Q.; Yin, N.-N.; Karsai, A.; da Rocha, S. R.; Liu, G.-y. High-Resolution Imaging of Polyethylene Glycol Coated Dendrimers via Combined Atomic Force and Scanning Tunneling Microscopy. *J. Drug Delivery* **2015,** *2015*.
41. Bielski, E. R.; Zhong, Q.; Brown, M.; da Rocha, S. R. Effect of the Conjugation Density of Triphenylphosphonium Cation on the Mitochondrial Targeting of Poly (amidoamine) Dendrimers. *Mol. Pharmaceutics* **2015,** *12*, (8), 3043-3053.
42. Speelmans, G.; Staffhorst, R. W.; de Kruijff, B.; de Wolf, F. A. Transport Studies of Doxorubicin in Model Membranes Indicate a Difference in Passive Diffusion across and Binding at the Outer and Inner Leaflet of the Plasma Membrane. *Biochemistry* **1994,** *33*, (46), 13761-13768.
43. de Wolf, F. A.; Staffhorst, R. W.; Smits, H. P.; Onwezen, M. F.; de Kruijff, B. Role of anionic phospholipids in the interaction of doxorubicin and plasma membrane vesicles: drug binding and structural consequences in bacterial systems. *Biochemistry* **1993,** *32*, (26), 6688-6695.
44. Kitchens, K. M.; Foraker, A. B.; Kolhatkar, R. B.; Swaan, P. W.; Ghandehari, H. Endocytosis and interaction of poly (amidoamine) dendrimers with Caco-2 cells. *Pharm. Res.* **2007,** *24*, (11), 2138-2145.
45. Jevprasesphant, R.; Penny, J.; Attwood, D.; D'Emanuele, A. Transport of dendrimer nanocarriers through epithelial cells via the transcellular route. *J. Controlled Release* **2004,** *97*, (2), 259-267.
46. De Duve, C.; De Barsy, T.; Poole, B.; Trouet, A.; Tulkens, P.; Van Hoof, F. Lysosomotropic agents. *Biochem. Pharmacol.* **1974,** *23*, (18), 2495-2531.
47. Kakinoki, A.; Kaneo, Y.; Ikeda, Y.; Tanaka, T.; Fujita, K. Synthesis of poly (vinyl alcohol)-doxorubicin conjugates containing cis-aconityl acid-cleavable bond and its isomer dependent doxorubicin release. *Biol. Pharm. Bull.* **2008,** *31*, (1), 103-110.
48. Minko, T.; Kopečková, P.; Pozharov, V.; Kopeček, J. HPMA copolymer bound adriamycin overcomes MDR1 gene encoded resistance in a human ovarian carcinoma cell line. *J. Controlled Release* **1998,** *54*, (2), 223-233.
49. Nance, E. A.; Woodworth, G. F.; Sailor, K. A.; Shih, T.-Y.; Xu, Q.; Swaminathan, G.; Xiang, D.; Eberhart, C.; Hanes, J. A dense poly (ethylene glycol) coating improves penetration of large polymeric nanoparticles within brain tissue. *Sci. Transl. Med.* **2012,** *4*, (149), 149ra119-149ra119.
50. Kutscher, H. L.; Chao, P.; Deshmukh, M.; Rajan, S. S.; Singh, Y.; Hu, P.; Joseph, L. B.; Stein, S.; Laskin, D. L.; Sinko, P. J. Enhanced passive pulmonary targeting and retention of PEGylated rigid microparticles in rats. *Int. J. Pharm.* **2010,** *402*, (1), 64-71.
51. Frezard, F.; Garnier-Suillerot, A. DNA-containing liposomes as a model for the study of cell membrane permeation by anthracycline derivatives. *Biochemistry* **1991,** *30*, (20), 5038-5043.

52. Kitchens, K. M.; Kolhatkar, R. B.; Swaan, P. W.; Ghandehari, H. Endocytosis inhibitors prevent poly (amidoamine) dendrimer internalization and permeability across Caco-2 cells. *Mol. Pharmaceutics* **2008,** *5*, (2), 364-369.
53. Albertazzi, L.; Serresi, M.; Albanese, A.; Beltram, F. Dendrimer internalization and intracellular trafficking in living cells. *Mol. Pharmaceutics* **2010,** *7*, (3), 680-688.
54. Seib, F. P.; Jones, A. T.; Duncan, R. Comparison of the endocytic properties of linear and branched PEIs, and cationic PAMAM dendrimers in B16f10 melanoma cells. *J. Controlled Release* **2007,** *117*, (3), 291-300.
55. Sahay, G.; Alakhova, D. Y.; Kabanov, A. V. Endocytosis of nanomedicines. *J. Controlled Release* **2010,** *145*, (3), 182-195.
56. Khakpoor, A.; Panyasrivanit, M.; Wikan, N.; Smith, D. R. A role for autophagolysosomes in dengue virus 3 production in HepG2 cells. *J. Gen. Virol.* **2009,** *90*, (5), 1093-1103.
57. Mohan, P.; Rapoport, N. Doxorubicin as a molecular nanotheranostic agent: effect of doxorubicin encapsulation in micelles or nanoemulsions on the ultrasound-mediated intracellular delivery and nuclear trafficking. *Mol. Pharmaceutics* **2010,** *7*, (6), 1959-1973.
58. Hillaireau, H.; Couvreur, P. Nanocarriers' entry into the cell: relevance to drug delivery. *Cell. Mol. Life Sci.* **2009,** *66*, (17), 2873-2896.
59. Lu, D.; Hickey, A. J. Pulmonary vaccine delivery. **2007**.
60. Stein, S. W.; Sheth, P.; Hodson, P. D.; Myrdal, P. B. Advances in metered dose inhaler technology: hardware development. *AAPS PharmSciTech* **2014,** *15*, (2), 326-338.
61. Jones, S. Suspension versus solution metered dose inhalers: different products, different particles? *J. Drug Delivery Sci. Technol.* **2011,** *21*, (4), 319-322.
62. Chokshi, U.; Selvam, P.; Porcar, L.; da Rocha, S. R. Reverse aqueous emulsions and microemulsions in HFA227 propellant stabilized by non-ionic ethoxylated amphiphiles. *Int. J. Pharm.* **2009,** *369*, (1), 176-184.
63. Wu, L.; da Rocha, S. R. Biocompatible and biodegradable copolymer stabilizers for hydrofluoroalkane dispersions: a colloidal probe microscopy investigation. *Langmuir* **2007,** *23*, (24), 12104-12110.
64. Conti, D. S.; Grashik, J.; Yang, L.; Wu, L.; da Rocha, S. R. Solvation in hydrofluoroalkanes: how can ethanol help? *J. Pharm. Pharmacol.* **2012,** *64*, (9), 1236-1244.
65. Myrdal, P. B.; Sheth, P.; Stein, S. W. Advances in metered dose inhaler technology: formulation development. *AAPS PharmSciTech* **2014,** *15*, (2), 434-455.
66. Reid, M. L.; Benaouda, F.; Khengar, R.; Jones, S. A.; Brown, M. B. Topical corticosteroid delivery into human skin using hydrofluoroalkane metered dose aerosol sprays. *Int. J. Pharm.* **2013,** *452*, (1), 157-165.
67. Peguin, R. P.; da Rocha, S. R. Solvent− solute interactions in hydrofluoroalkane propellants. *J. Phys. Chem. B* **2008,** *112*, (27), 8084-8094.
68. Wu, L.; Bharatwaj, B.; Panyam, J.; da Rocha, S. R. Core–shell particles for the dispersion of small polar drugs and biomolecules in hydrofluoroalkane propellants. *Pharm. Res.* **2008,** *25*, (2), 289-301.
69. Rogueda, P. G. HPFP, a model propellant for pMDIs. *Drug Dev. Ind. Pharm.* **2003,** *29*, (1), 39-49.
70. Stein, S.; Stefely, J. Reinventing metered dose inhalers: from poorly efficient CFC MDIs to highly efficient HFA MDIs. *Drug Deliv. Technol* **2003,** *3*, (1), 46-51.

71. Ostrander, K. D.; Bosch, H. W.; Bondanza, D. M. An in-vitro assessment of a NanoCrystal™ beclomethasone dipropionate colloidal dispersion via ultrasonic nebulization. *Eur. J. Pharm. Biopharm.* **1999,** *48*, (3), 207-215.
72. Leach, C.; Davidson, P.; Boudreau, R. Improved airway targeting with the CFC-free HFA-beclomethasone metered-dose inhaler compared with CFC-beclomethasone. *Eur. Respir. J.* **1998,** *12*, (6), 1346-1353.
73. Stefely, J. S. Novel excipients for inhalation drug delivery: expanding the capability of the MDI. *Drug Deliv. Technol.* **2002,** *2*, (6), 62-64.
74. Carvalho, T. C.; Peters, J. I.; Williams, R. O. Influence of particle size on regional lung deposition–what evidence is there? *Int. J. Pharm.* **2011,** *406*, (1), 1-10.